Received: 17 June 2025 | Accepted: 25 August 2025

DOI: 10.1002/tpg2.70124

The Plant Genome

ORIGINAL ARTICLE

Mapping novel yellow and leaf rust loci and predicting resistance in cross derived Canadian durum wheat

Juan Menor de Gaspar[1] | **Alejandro Domínguez Rondón**[1] | **Julián García-Abadillo**[1] | **Ron Knox**[2] | **Firdissa E. Bokore**[2] | **Kerry Boyle**[3] | **Karim Ammar**[4] | **Julio Huerta-Espino**[5] | **Samia Berraies**[2] | **Brad Meyer**[2] | **Wentao Zhang**[3] | **Richard D. Cuthbert**[2] | **Fobert Pierre**[3] | **Yuefeng Ruan**[2] | **Julio Isidro y Sánchez**[1]

[1]Centro de Biotecnologia y Genómica de Plantas (CBGP, UPM-INIA), Universidad Politécnica de Madrid (UPM)—Instituto Nacional de Investigación y Tecnologia Agraria y Alimentaria (INIA), Campus de Montegancedo-UPM, Madrid, Spain

[2]Swift Current Research and Development Centre, Agriculture and Agri-Food Canada, Swift Current, Saskatchewan, Canada

[3]Aquatic and Crop Resource Development, National Research Council of Canada, Saskatoon, Saskatchewan, Canada

[4]International Maize and Wheat Improvement Center, CIMMYT, Texcoco, México

[5]Campo Experimental Valle de México, INIFAP, Texcoco, México

Correspondence
Juan Menor de Gaspar and Julio Isidro y Sánchez, Centro de Biotecnologia y Genómica de Plantas (CBGP, UPM-INIA), Universidad Politécnica de Madrid (UPM)—Instituto Nacional de Investigación y Tecnologia Agraria y Alimentaria (INIA), Campus de Montegancedo-UPM, Pozuelo de Alarcón, Madrid, 28223, Spain.
Email: ju.martin@upm.es and j.isidro@upm.es
Yuefeng Ruan, Swift Current Research and Development Centre, Agriculture and Agri-Food Canada, Swift Current, Saskatchewan, Canada.
Email: yuefeng.ruan@agr.gc.ca

Assigned to Associate Editor Nonoy Bandillo.

Abstract

Durum wheat (*Triticum turgidum* ssp. *durum*) suffers substantial yield losses from yellow rust (*Puccinia striiformis*) and leaf rust (*Puccinia triticina*). In this study, we employed genome-wide association studies (GWAS) to identify loci associated with rust resistance and used genomic selection (GS) to evaluate the predictive accuracy of different statistical models and phenotyping metrics (`AUDPC_GDD`, `Angle`, `GDD50`, and `maxVar`) in a Canadian durum wheat panel. The panel was evaluated in Mexico for yellow rust across three seasons near Toluca, and for leaf rust over two seasons at El Batán. Our GWAS identified 36 significant marker-trait associations (MTAs), including known loci (*Yr30, Yr57, Yr82, YrU1, Lr16, Lr17, Lr18*, and *Lr65*) and previously unreported regions. Yellow rust resistance was linked to loci on chromosomes 3A (602.7 Mbp) and 3B (243.4 Mbp), while leaf rust MTAs appeared on chromosomes 5A (552.8 Mbp) and 7A (570 Mbp). Candidate genes near novel MTAs encode defense-related proteins such as serine/threonine kinases and NB-ARC (nucleotide binding–Apaf-1, R proteins, and CED-4), F-box, and RIN4 (RPM1-interacting

Abbreviations: AAFC, Agriculture and Agri-Food Canada; APR, adult-plant resistance; ASR, all-stage seedling resistance; AUDPC, area under the disease progress curve; BLUE, best linear unbiased estimator; BLUP, best linear unbiased predictor; CIMMYT, International Maize and Wheat Improvement Center; DH, doubled haploid; FHB, Fusarium head blight; GBLUP, genomic best linear unbiased predictor; GDDs, growing degree days; GO, Gene Ontology; GS, genomic selection; GWAS, genome-wide association study; LD, linkage disequilibrium; LEA, late embryogenesis abundant; LOD, logarithm of the odds; MTA, marker-trait association; NB-ARC, nucleotide binding–Apaf-1, R proteins, and CED-4; NLR, nucleotide-binding leucine-rich repeat; *Q–Q*,, quantile-quantile; QTL, quantitative trait loci; RIL, recombinant inbred line; RIN4, RPM1-interacting protein 4; RING, really interesting new gene; RKHS, reproducing kernel Hilbert spaces; SMR, SNP, single nucleotide polymorphism; WH2, WASP Homology.

Funding information
Government of Saskatchewan Agriculture Development Fund, Grant/Award Number: 20130015; Saskatchewan Wheat Development Commission, Grant/Award Number: 171025-63; Agriculture and Agri-Food Canada; Canadian National Wheat Cluster program; Canadian Wheat Research Coalition; MCIN/AEI/10.13039/501 100 011 033, Grant/Award Number: PID2021-123718OB-I00; ERDF A way of making Europe, Grant/Award Number: CEX2020-000999-S; National Research Council of Canada

protein 4)-domain proteins. Among four scoring metrics tested, `AUDPC_GDD` consistently outperformed others for yellow rust, whereas `maxVar` was most effective for leaf rust, reflecting differences in phenotypic distribution and trait variance. Bayesian GS models (BayesB) achieved the highest prediction accuracy, but including GWAS-derived fixed effects did not improve predictions, likely due to complexities in modeling major-effect loci. These results underscore the importance of rust-specific phenotyping strategies and illustrate the difficulty of integrating GWAS into GS models to dissect complex resistance traits.

Plain Language Summary

Durum wheat, a staple crop used for commodities like pasta and couscous, faces significant yield losses from fungal diseases like yellow and leaf rust. Our study focused on finding the best methods for the genetic analysis of rust resistance. We used a mapping analysis (GWAS) to pinpoint 36 genetic markers–including both known resistance genes and newly discovered regions–and then tested which of four disease-scoring metrics was most effective. We also investigated if adding these top markers could improve resistance predictions (Genomic Selection). Our results showed that the ideal metric depends on the specific rust disease, and while a BayesB model was most accurate for prediction, incorporating the markers did not enhance its performance. This research provides clear guidance on effective methods, helping breeders accelerate the development of more durable, rust-resistant durum wheat.

1 | INTRODUCTION

Wheat (*Triticum* spp.) is a major staple worldwide, supplying a substantial share of human caloric intake (Mottaleb et al., 2023). Durum wheat (*Triticum turgidum* ssp. *durum*) is especially important for pasta and semolina, underpinning economies in many regions (Martínez-Moreno et al., 2020). However, prevalent fungal diseases—particularly yellow rust (*Puccinia striiformis* f. sp. *tritici*) and leaf rust (*Puccinia triticina* Erikss.), continue to threaten global wheat production (W. Chen et al., 2014; Prasad et al., 2020; Savary et al., 2019; Wellings, 2011).

In 2010, yellow rust epidemics in the Middle East and North Africa caused yield losses of up to 80% (Solh et al., 2012). Leaf rust typically reduces yields by 15%–50%, with total crop failure under severe outbreaks (Dubin & Rajaram, 1996; Savary et al., 2019). Recent epidemics in North Kazakhstan, Iran, and Africa highlight the urgency of effective disease management (Genievskaya et al., 2020; Talebi et al., 2023) (https://rusttracker.cimmyt.org).

Researchers have invested extensive effort in combating rust. Although fungicides work well, they pose environmental risks and can hasten fungicide-resistant strains (Figlan et al., 2020). Breeding resistant cultivars offers a more sustainable option (Dong et al., 2017; Qiao et al., 2024; Talebi et al., 2023), and over 80 major *Yr* and *Lr* genes have been identified to date (X. Chen, 2020; S. Huang et al., 2021; McIntosh et al., 1995; Prasad et al., 2020).

Genetic resistance is divided into all-stage seedling resistance (ASR) and adult-plant resistance (APR) (Bouvet et al., 2021; D. Kumar et al., 2020). ASR is race-specific and governed by single major genes (e.g., *Yr5*, *Yr15*, *Lr76*, *Lr80*) that protect plants throughout their life but often succumb to evolving pathogen races (M. Bansal et al., 2016; S. Kumar et al., 2021; Yao et al., 2021). By contrast, APR confers partial, non-race-specific resistance via multiple minor-effect genes (e.g., *Yr36*, *Lr34/Yr18*, *Lr46/Yr29*, *Lr67/Yr46*), many encoding nucleotide-binding leucine-rich repeat (NLR) proteins essential for plant immunity (Hiebert et al., 2010; Prasad et al., 2020; Qiao et al., 2024; Singh et al., 1998).

Genome-wide association studies (GWAS) have greatly clarified the genetic basis of rust resistance by pinpointing key loci through historical recombination in diverse germplasm panels (Aoun et al., 2021; Desiderio et al., 2014; Sapkota et al., 2019). Many quantitative trait loci (QTL) for rust map to all durum wheat chromosomes, often co-localizing with known *Lr* and *Yr* genes or marking novel regions (Aoun et al., 2016; Alemu et al., 2021; Aoun et al., 2021; Liu et al., 2016; Yao et al., 2021). These findings underscore GWAS as a powerful tool to harness genetic variation for breeding.

Combining GWAS with genomic selection (GS) can speed resistance breeding (Mahmood et al., 2022; Spindel et al.,

2016). GS uses genome-wide markers to predict breeding values, enabling faster selection and shorter cycles (Heffner et al., 2010; Isidro et al., 2016; Meuwissen et al., 2001), especially for polygenic traits (Klymiuk et al., 2023). Merging GWAS and GS helps pinpoint and validate key loci while boosting selection accuracy (Bernardo, 2014; Rutkoski et al., 2014; Spindel et al., 2016).

High-quality phenotypic data are crucial for reliable GWAS and GS, given the complexity of genotype–environment interactions. Collaborative trial networks (e.g., International Maize and Wheat Improvement Center (CIMMYT), Borlaug Global Rust Initiative, and WheatSustain) gather multiyear, multilocation data, creating robust datasets for accurate modeling. Yet, standardizing protocols remains challenging (Akdemir et al., 2020), as assessment frequency and timing can skew measurements. Rigorous scoring methodologies are therefore vital for consistent cross-trial comparisons.

Area under the disease progress curve (AUDPC) is a widely used metric that integrates disease progression with plant growth (Jeger & Viljanen-Rollinson, 2001; Thompson & Silverman, 2008). However, it has following drawbacks: (i) it demands multiple assessments spanning the entire disease cycle, (ii) yields unconventional units that complicate interpretation, and (iii) introduces potential bias if the timing or frequency of assessments is uneven. Consequently, identical disease trajectories can yield starkly different AUDPC scores.

Addressing these limitations, Garcia-Abadillo et al. (2023) developed more efficient scoring metrics that optimize information from each assessment, reduce the burden of exhaustive phenotyping, and enable fair comparisons across Fusarium head blight (FHB) trials. These novel approaches have lowered phenotyping costs without compromising predictive accuracy. Building on these advances, we sought to adapt similar strategies for rust phenotyping in Canadian durum wheat, aiming to uncover new associations and refine selection tools. Here, we explore novel associations for yellow and leaf rust resistance in durum wheat lines from a public Canadian breeding program. Our objectives are twofold: (i) to identify new genomic regions linked to rust resistance and (ii) to evaluate and compare alternative phenotyping metrics and genomic prediction models for breeding rust-resistant durum wheat. By integrating GWAS findings with advanced GS, we aim to develop more robust rust-resistant cultivars.

2 | MATERIALS AND METHODS

2.1 | Plant materials

This study utilized a diverse panel of durum wheat lines, parents, and checks, consisting of 372 recombinant inbred lines (RILs) and 98 doubled haploid (DH) lines (Table 1). RILs were developed by Dr. Ron Knox in 2012 at Agriculture and Agri-Food Canada's (AAFC) Swift Current Research and Development Centre via biparental crosses and single-seed descent. Four hexaploid wheat donors, HY644-BE, BW871, P89-77-1B, and Sumai-3, were crossed to durum wheat parents (DT833, Transcend, DT801, DT818, and Langdon) (Joppa & Williams, 1988) to introgress FHB resistance. F_1 and F_2 progeny were genotyped with markers flanking the three major FHB QTL resistant loci, and lines were advanced through to the F_9 generation by single-seed descent. The resulting RILs were then evaluated for leaf rust and stripe rust resistance. The DH population, A0560& (A0100B-005/A9831-DC*1), comprising 98 lines, was derived from the F_1 hybrid of durum wheat using the wheat × maize hybridization method described by Knox et al. (2000). A0100B-005, introduced from Germany, served as one of the parental lines.

2.1.1 | Yellow rust evaluation

Yellow rust evaluations were conducted at the CIMMYT Mexico Tuluca experimental station in 2018, 2019, and 2022 (Figure 1A), in a randomized block design with two replications (Figure 1B). The lines were grown in single rows, each 1.5 m long, with 30 seeds per row. Spreader rows were inoculated with the purified MX16-04 race, which spread onto spreader rows of susceptible wheat varieties and across each plot. The inoculation process involved three successive applications of highly concentrated inoculum suspended in Soltrol during mid-August. Each year, the percentage of yellow rust-infected area on the uppermost leaves was assessed four to five times, with 7- to 10-day intervals between assessments (Figure 1C).

2.1.2 | Leaf rust evaluation

Leaf rust evaluations were conducted at the CIMMYT Mexico experimental station, El Batán, during 2018 and 2019 (Figure 1A). Trials were arranged in single rows, each measuring 1.5 m in length, following a randomized complete block design with two replications (Figure 1B). Although identical genotypes were sown at both sites, line failures in Toluca and the inclusion of the parental lines Langdon and A0100B-005 yielded a slightly different final count of unique genotypes. Artificial inoculation using the Cirno race (BBG/BP), which exhibits additional virulence against LrCamayo (Herrera-Foessel et al., 2007), was employed to ensure disease pressure throughout the 2 test years. All lines of the A0560& cross demonstrated susceptibility to the Mexican races inoculated, resulting in no variation among the lines for QTL analysis. Consequently, the evaluations were not repeated with RILs in subsequent years. Each year, the percentage (%) of leaf rust-infected area on the uppermost leaves was assessed four to five times, with 7- to 10-day intervals between assessments (Figure 1C).

TABLE 1 Summary of tested populations.

Cross	Population type	Pedigree	Number of lines	Leaf rust	Yellow rust
A1290C	RIL	DT833//P89-77-1B/Sumai-3	3	El Batán	Toluca
A1293C	RIL	DT833//HY644-BE/Transcend	29	El Batán	Toluca
A1293D	RIL	DT818//HY644-BE/Transcend	43	El Batán	Toluca
A1293E	RIL	DT844//HY644-BE/Transcend	255	El Batán	Toluca
A1294C	RIL	DT833//BW871/Langdon	42	El Batán	Toluca
A0560&	DH	A0100B-005/A9831-DC*1	98	El Batán	Toluca
Total			470		

Note: Description of a panel comprising recombinant inbred lines (RILs) derived from durum × hexaploid × durum crosses and a doubled haploid (DH) population of durum wheat, evaluated for resistance to leaf rust and yellow rust in Mexico.

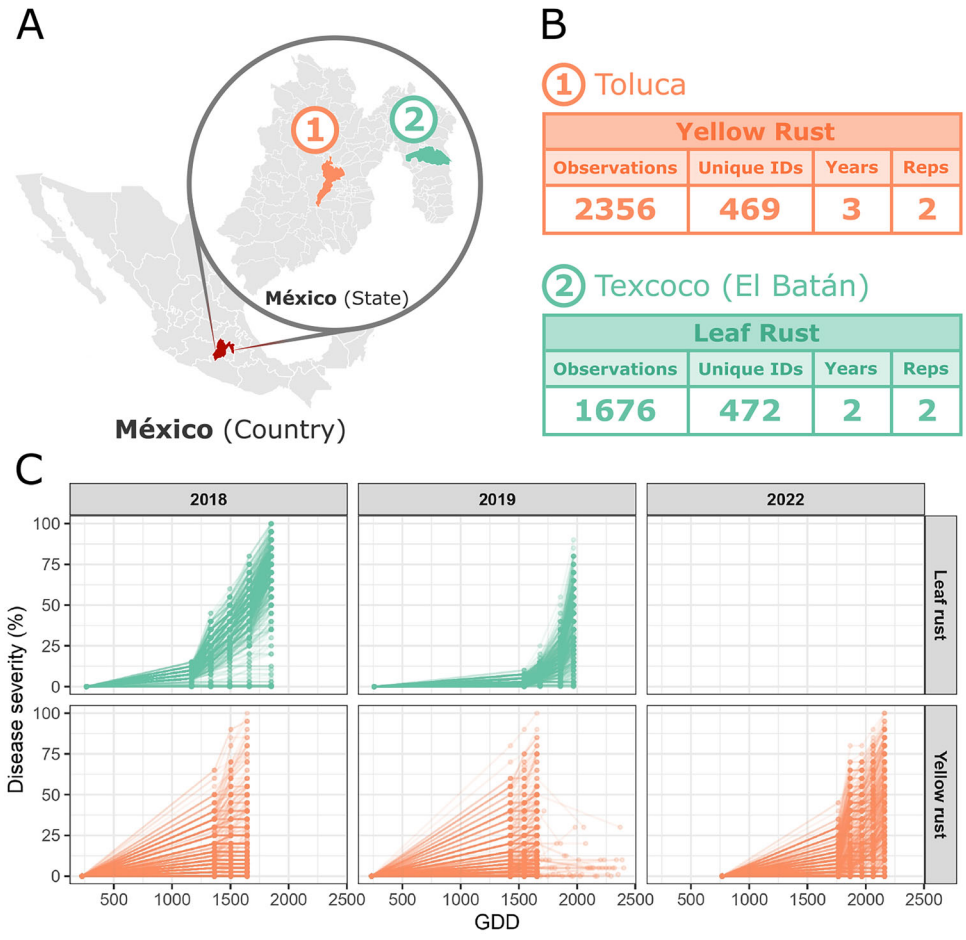

FIGURE 1 Summary of phenomic data. (A) Geographical location of trials. (B) Summary tables providing key information about the trials. (C) Disease severity (%) versus the accumulated growing degree days (GDDs; Section 2.3) for each measured year and disease.

2.2 | Genotyping

Genomic data for the A129X cross were generated using *TraitGenetics 25K SNP array*, while the *Illumina 90K iSelect Wheat SNP array* was employed for the A0560& cross. A total of 10,919 single nucleotide polymorphisms (SNPs) were common to both arrays and retained for analysis. Processing of these SNPs was performed manually using `R` (4.4.1) (R Core Team, 2024), and imputation using the `rrBLUP` package (4.6.3) (Endelman, 2011) with an expectation maximization algorithm (Poland et al., 2012). Monomorphic SNPs and those with a minor allele frequency below 0.05 were filtered out. After filtering, 10,491 SNPs remained. For analysis, nucleotide letters were converted into allele dosages (0, 1, and 2), representing the dosage of the minor allele.

2.3 | Scoring metrics

Scoring metrics and AUDPC calculation were performed as described in Garcia-Abadillo et al. (2023). To include temperature effects on plant growth and disease development and to account for environmental variation across environments, the AUDPC and the other alternative disease scores were computed using growing degree days (GDDs) as the thermal time units as described in McMaster (1997). Accumulated GDDs were computed as follows per year and location:

$$\begin{cases} \text{GDD}_{(0)} = 0 \\ \text{GDD}_{(t)} = \text{GDD}_{(t-1)} + \max\left[0, \left(\frac{T_{\max(t)}+T_{\min(t)}}{2} - T_{\text{base}}\right)\right] \end{cases}$$

where $\text{GDD}_{(t)}$ is the value of accumulated GDDs on the tth day, $T_{\max(t)}$ and $T_{\min(t)}$ are respectively the maximum and minimum temperatures recorded on the tth day, and T_{base} is the fixed threshold to increment GDDs. T_{base} was set to 0°C in this study for all locations.

The AUDPC was therefore measured using these GDDs as the time dimension, so from now on we refer to this metric as `AUDPC_GDD` (`AUDPC` normalized by GDD).

The proposed three alternative scoring metrics adhere to the following formulation: Let $X = \{x_1, x_2, \ldots, x_T\}$ be the set of accumulated GDDs from anthesis corresponding to the T assessment's dates and $Y = \{y_1, y_2, \ldots, y_T\}$ the set of T rust severity evaluations. The resulting scoring metric was defined (Garcia-Abadillo et al., 2023) as a function that maps X and Y into a score to be used as the response variable in further analysis. For clarity, a graphical representation of the following metrics is presented on Figure 2.

2.3.1 | Angle

The advantage of this metric is that it can be used with as little as one data point. It's calculated applying the *arctan* function on the slope computed between a single assessment (x_T, y_T) and the origin (0,0) measured in degrees. Or more precisely, between the average time value in which disease severity reaches the final plateau and the origin:

$$\begin{cases} \text{Angle}(X, Y) = arctan\left(\frac{y_T}{\frac{x_p+x_T}{2}}\right) \\ x_p = min(X \,|\, y = y_T) \end{cases}$$

where x_p is the minimum value of X given that the maximum value of disease severity (y_T) is reached, that is, the first time that the maximum disease reached was recorded. An earlier and higher peak severity steepens the origin to peak trajectory, yielding a larger angle that signifies more rapid and severe disease progression.

2.3.2 | GDD50

This metric was defined as the accumulated GDDs in which a plot reaches 50% of the total disease severity. Also described as the latent period in disease progression in the literature (Das et al., 1993), this metric has also been used as a parameter to characterize partial disease resistance. It can be calculated by linear interpolation as follows:

$$\begin{cases} \text{GDD50}(X, Y) = \frac{50-y_L}{y_R-y_L}(x_R - x_L) + x_L \\ \begin{cases} L = \text{argmax}_x(X \,|\, y \le 50) \\ R = \text{argmin}_x(X \,|\, y \ge 50) \end{cases} \end{cases}$$

where L and R are the indexes of the closest points (to the left and right, respectively) to the target disease level (50%), so (x_L, y_L) and (x_R, y_R) are the best points to linearly interpolate `GDD50`.

2.3.3 | Maximum variance

This score is measured as the percentage of disease severity with the highest variability among lines in the disease severity assessment. Mathematically, this is expressed as:

$$\begin{cases} \text{maxVar}(X, Y) = y_{\text{rust\_max}} \\ \text{rust\_max} = \text{argmax}_t \left[\sum_{i=1}^{N}\left(\text{RUST}_{it} - \overline{\text{RUST}}_{.t}\right)^2\right] \end{cases}$$

where RUST is an $N \times T$ matrix with RUST_{it} being the disease value for ith plot and tth assessment, $\overline{\text{RUST}}_{.t}$ is the mean disease value in the tth assessment, and maxVar is maximum variance. Thus, rust_max is the highest variability assessment index. This metric is easy to measure but requires the phenotypic information of all lines before computing it.

2.4 | Genome-wide association study

A mixed linear model (Equation 1) was fitted for each scoring metric using the `lme4` package (1.1-37) (Bates et al., 2015) to consolidate repeated measurements across years. In this model, a disease severity metric serves as the response variable, with genotype, year, plant height (PH), and heading date (HD) included as fixed effects, while the repetition nested within the year was modeled as a random effect. PH) and HD) were incorporated as covariates only when their inclusion minimized the Akaike information criterion value as previous work has shown that including these traits boosts predictive accuracy via their association with disease resistance (Garcia-Abadillo et al., 2023). For the leaf rust disease, covariates were used in all cases except for the `Angle`

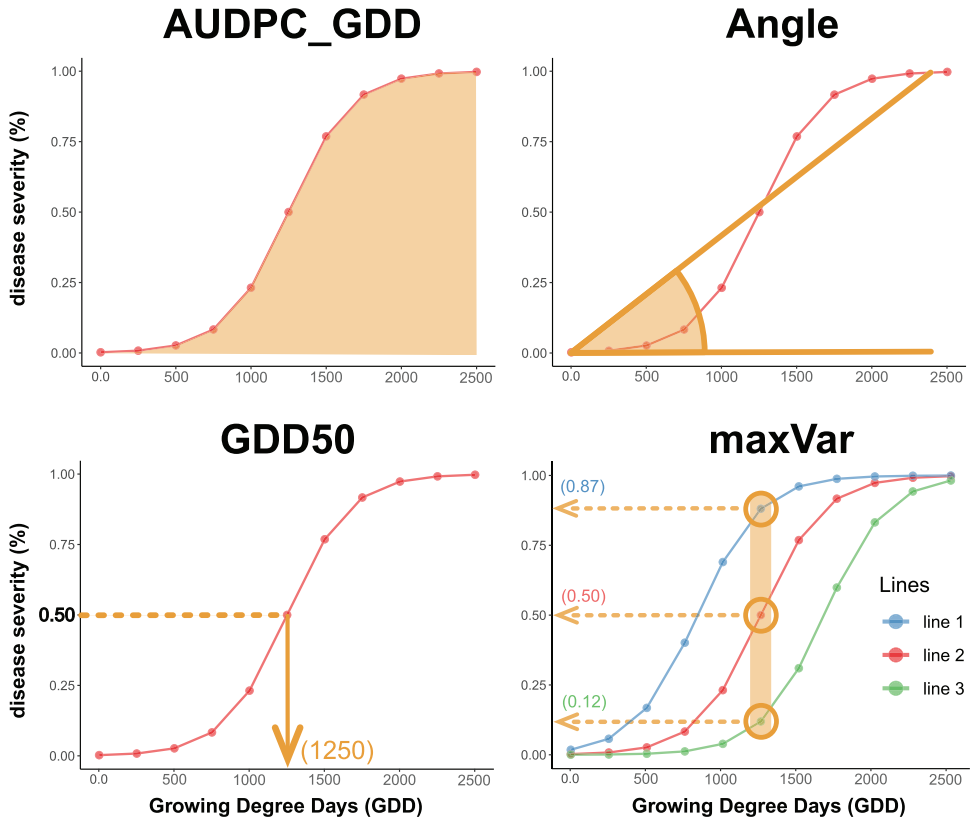

FIGURE 2 Graphical representation of scoring metrics: `AUDPC_GDD` (top left): The area under the disease progress curve (`AUDPC`) calculated based on growing degree days (`GDD`), shown as the shaded region. `Angle` (top right): The angle formed between the maximum disease severity and the origin. `GDD50` (bottom left): The `GDD` value at which disease severity reaches 50%. `maxVar` (bottom right): The disease severity value measured on the assessment with higher variation between lines.

metric, which utilized only the HD; in contrast, for the yellow rust disease, only the `AUDPC_GDD` metric employed the PH covariate, while the remaining metrics did not use any additional covariates. Finally, the resulting genotype best linear unbiased estimators (BLUEs) were used as the response variable for the subsequent genome-wide association study (GWAS).

We employed the R package `GAPIT` (3.5) (R Core Team, 2024; J. Wang, 2024) to perform GWAS using the Bayesian information and linkage-disequilibrium iteratively nested keyway method (M. Huang et al., 2018). To correct for population structure, a kinship matrix and principal components (PCs) were included in the model. The optimal number of PCs was determined by evaluating the variance explained by each one and assessing model fit using quantile-quantile (*Q*–*Q*) plots for models with an increasing number of PCs. We selected the first three PCs, as they captured the majority of the population structure and effectively controlled for *p*-value inflation, with no significant improvement from including additional components (Larsson et al., 2013). To minimize type I error rates, *p*-values were adjusted using the Bonferroni correction (0.05/number of SNPs). Visualization of the results was carried out using Manhattan and *Q*–*Q* plots, generated with the R package `CMplot` (4.5.1) (Yin et al., 2021), to confirm the final model fit.

$$y = X_g\, g + X_{\text{year}}\, \text{year} + \left[X_{\text{PH}}\text{PH} + X_{\text{HD}}\text{HD}\right] + Z_{\text{rep}}\, \text{year(rep)} + \epsilon \quad (1)$$

where:

- y is a vector of disease severity score metric values;
- g is a vector of BLUEs for the fixed genotypic effect;
- year is a vector of BLUEs for the fixed year effect;
- $\text{year(rep)} \sim N(0, I\sigma^2_{\text{year(rep)}})$ is a vector of best linear unbiased predictors (BLUPs) for the random effect of the repetition nested within the year;
- PH and HD are the two coefficients associated with the effect of plant height and heading date, respectively. Expressed between square brackets to indicate that these terms may be included or omitted depending on the scenario;
- X_g, X_{year}, X_{PH}, X_{HD}, and Z_{rep} are the design matrices of their corresponding effects;
- $\epsilon \sim N(0, I\sigma^2_{\epsilon})$ is the residual.

2.5 | Linkage disequilibrium analysis

We estimated pairwise linkage disequilibrium (LD), measured as r^2, among all genotyped markers. To determine the extent of LD decay, we identified the average physical distance at which r^2 dropped below a threshold of 0.2. This empirically derived distance was then used to define a uniform window for interpreting GWAS results; any significant peak located within this distance of a previously reported signal or candidate gene was considered to tag the same underlying locus. This strategy aligns with previous analyses in this population, enhances reproducibility, and avoids the parameter tuning required by haplotype-block algorithms. Future studies could leverage block-calling methods to investigate local LD structure more thoroughly. All LD calculations were performed using the `LD.decay` function implemented in the R package `sommer` (4.3.5) (Giovanny, 2016).

2.6 | Candidate gene identification and functional annotation

We identified all SNP markers exceeding the significance threshold ($\alpha = 0.05/10,492$, LOD > 5.32, where LOD is logarithm of the odds) as candidate loci. Candidate genes located within 50 kb of these significant markers were retrieved from the durum wheat reference genome (`cv. Svevo RefSeq Rel.1.0`) (Maccaferri et al., 2019).

To investigate the biological relevance of these genes, we queried the UniProt database (The UniProt Consortium, 2022) using its application programming interface. This allowed us to obtain associated protein information and predict possible gene functions by analyzing corresponding Gene Ontology (GO) annotations (Ashburner et al., 2000; The Gene Ontology Consortium et al., 2023), following approaches previously described in the literature (García-Abadillo et al., 2024; Lebrec et al., 2009).

We calculated GO-based correlations between disease metrics using the Jaccard similarity index, whereas phenotype-based correlations were computed as Pearson correlations. All analyses were performed in `R` (R Core Team, 2024), using the packages `ggplot2` (3.5.1) (Wickham, 2016), `ggraph` (2.2.1) (Pedersen, 2024a), `tidygraph` (1.3.1) (Pedersen, 2024b), and `dplyr` (1.1.4) (Wickham et al., 2023) for data processing and visualization.

2.7 | GS assay

For each disease, we randomly partitioned the entire dataset into 70% training and 30% test sets. We first performed GWAS on the training set following the methods described in Section 2.4. Next, we fitted three genomic prediction models (genomic best linear unbiased predictor [GBLUP], BayesB, and reproducing kernel Hilbert spaces [RKHS]) under three scenarios: (1) using only marker data from the training set (without GWAS hits), (2) incorporating significant GWAS hits identified in the training set as fixed effects, and (3) incorporating significant GWAS hits identified from the entire dataset as fixed effects (positive control). This approach was replicated 60 times per scenario with different training/test splits to minimize the impact of random variability in the results, ensuring a robust evaluation by reporting the mean prediction accuracy across these replicates.

We then predicted the phenotypes of the test set and quantified the prediction accuracy as the Pearson correlation between predicted values (line BLUPs plus SNP fixed effects when included) and adjusted observed phenotypes. The GBLUP model was fitted with the `sommer` package (Giovanny, 2016), whereas we implemented BayesB and RKHS models using the `BGLR` package (1.1.2) (Pérez & de los Campos, 2014).

2.7.1 | GBLUP model

The mixed model for GBLUP is given by Equation (2):

$$g = \left[\mu + X\,\text{snps}\right] + Z_u\,u + \epsilon, \tag{2}$$

where:

- g is the vector of genotypic BLUEs computed in Equation (1);
- μ is the overall intercept;
- snps is the vector of fixed effects for the GWAS hits;
- $u \sim N(0, G\sigma_u^2)$ is the vector of random additive genotypic effects following VanRaden's genomic relationship matrix G (VanRaden, 2008);
- X and Z_g are the design matrices for the fixed and random effects, respectively;
- $\epsilon \sim N(0, I\sigma_\epsilon^2)$ is the residual error.

The notation $\left[\mu + X\text{snps}\right]$ indicates that these fixed effects are included when GWAS hits are incorporated. When modeling without GWAS hits, only the intercept μ is present.

2.7.2 | BayesB model

The BayesB model follows a similar structure but replaces the random additive genomic effect u with individual marker effects β_j drawn from a prior distribution that allows most markers to have zero effect while a subset may have large

nonzero effects:

$$\beta_j \sim \begin{cases} 0 & \text{with probability } \pi \\ N(0, \sigma^2_{\beta_j}) & \text{with probability } 1-\pi \end{cases}$$

with $\sigma^2_{\beta_j} \sim \chi^{-2}(\upsilon, S^2)$, and where π, ν, and S^2 are hyperparameters defined by default in the package (Pérez & de los Campos, 2014).

2.7.3 | RKHS model

For the RKHS regression model, instead of selecting a single bandwidth parameter h for the Gaussian kernel via cross-validation or Bayesian methods (both computationally demanding), we adopted the multi-kernel approach (kernel averaging) suggested by De Los Campos et al. (2010). In this approach, a sequence of kernels is defined based on a set of reasonable values of h, and then a model is fitted with all of these kernels as random effects (Pérez & de los Campos, 2014). This procedure is equivalent to a model with a single random effect whose distribution is a weighted average of all the kernels used, with weights proportional to the corresponding variance components. We chose the following seven values for h to cover the entire range of optimal values that we saw were possible with our data:

$$h = \left\{\frac{1}{6}, \frac{1}{4}, \frac{3}{8}, \frac{1}{2}, \frac{3}{4}, 1, \frac{3}{2}\right\}$$

A Gaussian kernel is defined as follows:

$$K(x_i, x_{i'}) = \exp\left\{-h \times \frac{\sum_{k=1}^{p}(x_{ik} - x_{i'k})^2}{p}\right\}$$

where x_i and $x_{i'}$ are the genotype vectors for individuals i and i', and p is the number of markers. This model follows the same general structure as both previous models (Equation 2) but the random additive genotypic term (u) is instead replaced by a sum of seven random genotypic terms ($\sum_{l=1}^{7} g_l$) that capture all genomic effects, not just additive, each one following:

$$p(g_1, \ldots, g_7) \propto \prod_{l=1}^{7} N(g|0, K_l\sigma^2_{g_l})$$

Variance components for the GBLUP model were estimated via restricted maximum likelihood, while both BayesB and RKHS used a Markov chain Monte Carlo approach with 25,000 iterations, discarding the first 5000 as burn-in. When GWAS hits were modeled as fixed effects, all models excluded these markers from the computation of their corresponding genotypic effect. This prevented the same marker from being treated simultaneously as both a random and a fixed effect.

3 | RESULTS

3.1 | Exploratory analysis

3.1.1 | Disease phenotype distributions

Figure 3 shows that none of the raw disease-severity metrics follow a standard distribution, likely reflecting strong year and year × genotype effects. For leaf rust, `GDD50` and `AUDPC_GDD` are distinctly bimodal, with a dip near the population mean, whereas `Angle` and `maxVar` are right-skewed, concentrating density above the mean.

Figure 3 shows that for yellow rust, all metrics are skewed below the mean. `AUDPC_GDD`, `Angle`, and `maxVar` share a broadly similar left-skewed profile, while `GDD50` stands out with a pronounced high-density peak below the mean and a smaller secondary peak above it. Compared to yellow rust, mean values for every metric are higher in leaf rust, indicating overall greater resistance to yellow rust, whereas yellow rust metrics (except `maxVar`) exhibit higher standard deviations.

Figure 8C shows no correlation between the two diseases. Within each disease, `AUDPC_GDD`, `Angle`, and `maxVar` are positively correlated, and `GDD50` is inversely correlated with the others. Leaf rust traits consistently display lower coefficients of variation (CV) and broad-sense heritabilities (H^2) than their yellow rust counterparts. Across both diseases, `GDD50` has the lowest CV and H^2, while `Angle` and `maxVar` yield the highest heritabilities (with yellow rust's `AUDPC_GDD` heritability matching that of `Angle`). `AUDPC_GDD` shows the highest CV in both pathosystems.

3.1.2 | Population structure and genetic relationships

The principal component analysis plot (Figure 4A) clearly distinguishes DH cross A0560& from the rest of the population, a result further supported by clustering analysis. Based on hierarchical clustering, we separated the remaining groups into seven clusters.

The first PC separates cross A0560& and parent A0100B-005 from the rest of the groups, accounting for 14.9% of the variability.

Clusters 5, 6, 7, and 8 collectively represent cross A1293E. These clusters share a similar Euclidean genetic distance, comparable to that observed among Clusters 2, 3, and 4.

Specifically, Cluster 2 contains exclusively individuals from cross A1293C. Cluster 3 primarily comprises individuals from cross A1294C. Cluster 4 includes all individu-

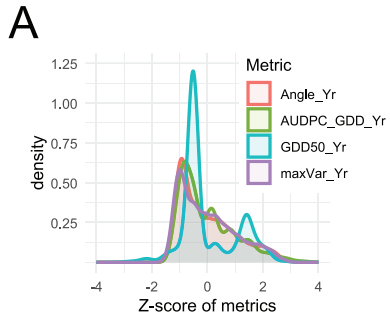

Yellow Rust					
Metric	Mean	Std	Range	CV	H^2
Angle	1.25	1.03	0.03 — 4.25	0.82	0.93
AUDPC_GDD	15165.3	12826.18	53.88 — 68023.2	0.85	0.93
GDD50	1785.73	265.97	980.73 — 2550.83	0.15	0.82
maxVar	32.34	25.37	0 — 100	0.78	0.89

Leaf Rust					
Metric	Mean	Std	Range	CV	H^2
Angle	1.96	0.99	0.03 — 3.61	0.51	0.87
AUDPC_GDD	19171.13	12389.83	200 — 48102.65	0.65	0.69
GDD50	1814.75	180.58	1332.22 — 2251.12	0.10	0.51
maxVar	55.49	27.34	1 — 100	0.49	0.88

FIGURE 3 Distribution and statistics of calculated scoring metrics: density plot of standardized *Z*-scores (left) and summary statistics (right) for yellow rust (A) and leaf rust (B). The accompanying statistics summarize the mean, standard deviation (Std), range, coefficient of variation (CV), and broad-sense heritability (H^2) (calculated using the Cullis method) for each metric. Correlations between them are available in Figure 8C.

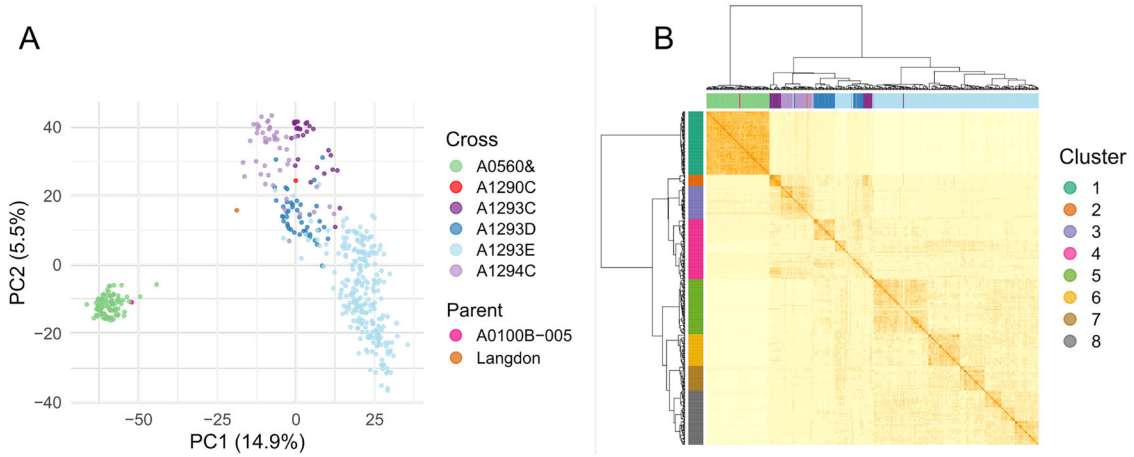

FIGURE 4 Principal component analysis and genomic relationship matrix. (A) Scatter plot showing each individual as a point, positioned based on their marker data. Points are colored according to their respective cross, allowing visual differentiation among them. (B) Heat map displaying the additive correlations between all individuals, with values represented on a color gradient from white (lowest correlation) to dark red (highest correlation). Individuals are arranged along both rows and columns using agglomerative hierarchical clustering, applying the Euclidean distance metric and Ward's agglomeration method. Distinct colors along the rows and columns indicate each individual's cross and cluster. The number of clusters was chosen to represent the patterns observed in the heatmap. Clustering is more clearly displayed in Figure S1.

als from cross A1293D, some individuals from A1293E, approximately half from A1293C, and two individuals from A1294C.

Figure S1 provides additional visualizations of the population structure, including a PC plot color-coded by cluster and a dendrogram illustrating the hierarchical clustering results.

In addition, the LD analysis showed that the average correlation (r^2) between markers decayed below 0.2 at a physical distance of approximately 12.5 Mbp (Figure S2), consistent with previous reports on LD decay in wheat (Somers et al., 2007).

3.2 | Genome-wide association analyses

We identified 36 significant associations surpassing the Bonferroni threshold ($\alpha = 0.05/10,492$, LOD > 5.32), comprising 20 associations for yellow rust and 16 for leaf rust,

TABLE 2 Genome-wide association study (GWAS) results: Significant marker-trait associations (MTAs) including the disease (yellow rust and leaf rust), the chromosome (Chr), the marker position, the logarithm of the odds (LOD: $-\log_{10}$ of the *p*-value), minor allele frequency (MAF), slope estimated by the model (Effect), and captured genotypic variance (R^2). The metric column indicates which scoring metric do the following statistics (LOD, Effect, and R^2) belong to. For a complete list with the statistics of all metrics and associated genes, see Table S2.

Disease	SNP	Chr	Position (bp)	MAF	Metric	LOD	Effect	R^2
Yellow	AX-95235178	1A	492,254,231	0.36	GDD50	7.76	18.13	0.02
Yellow	wsnp_BE494527A_Ta_2_1	1A	538,665,173	0.07	AUDPC_GDD	12.53	3873.48	0.10
Yellow	AX-89391029	2B	765,142,692	0.18	GDD50	6.26	−22.48	0.13
Yellow	Tdurum_contig52627_726	2B	767,717,188	0.40	AUDPC_GDD	5.60	−1454.24	0.02
Yellow	wsnp_Ex_c8884_14841846	3A	602,725,305	0.26	AUDPC_GDD	9.28	−2135.93	0.04
Yellow	AX-94591477	3B	3,057,551	0.46	Angle	6.03	−0.13	0.14
Yellow	IACX5776	3B	5,563,727	0.25	AUDPC_GDD	5.97	−1583.08	0.04
Yellow	TA011763-0791	3B	72,695,676	0.35	AUDPC_GDD	5.53	1205.09	0.01
Yellow	AX-158541430	3B	243,418,450	0.50	AUDPC_GDD	7.73	−2009.67	0.02
Yellow	GENE−2105_409	3B	754,481,869	0.06	AUDPC_GDD	8.90	4283.06	0.15
Yellow	Excalibur_c29568_163	4B	650,637,990	0.06	AUDPC_GDD	8.70	−3399.92	0.01
Yellow	BobWhite_c17440_130	5A	398,114,150	0.06	AUDPC_GDD	6.07	−3315.38	0.02
Yellow	Excalibur_c100531_251	5A	563,166,503	0.35	GDD50	6.03	17.56	0.00
Yellow	IAAV5779	5A	607,912,328	0.20	AUDPC_GDD	9.13	−2258.63	0.04
Yellow	BS00093522_51	5B	568,153,025	0.19	AUDPC_GDD	7.16	2242.05	0.07
Yellow	BobWhite_c16916_658	5B	682,388,260	0.37	GDD50	19.66	−37.77	0.22
Yellow	BS00097030_51	5B	684,349,754	0.38	Angle	23.00	0.36	0.34
Yellow	Tdurum_contig84832_110	5B	684,351,950	0.39	AUDPC_GDD	33.08	5185.22	0.37
Yellow	Excalibur_c43044_385	7A	52,378,527	0.22	AUDPC_GDD	6.28	1904.89	0.11
Yellow	Excalibur_c51720_84	7A	709,197,505	0.18	AUDPC_GDD	5.45	1767.57	0.01
Leaf	Tdurum_contig10208_447	2A	296,706	0.09	AUDPC_GDD	5.73	−2289.73	0.15
Leaf	Tdurum_contig11802_864	2B	2,559,891	0.06	AUDPC_GDD	10.50	−3812.98	0.16
Leaf	IAAV1798	2B	776,456,231	0.32	Angle	6.65	0.18	0.05
Leaf	AX-158578056	3B	588,705,723	0.35	Angle	5.88	0.40	0.01
Leaf	AX-94849518	3B	595,084,873	0.15	Angle	6.92	−0.46	0.07
Leaf	AX-158579240	3B	795,460,650	0.05	Angle	5.52	0.21	0.01
Leaf	AX-94721806	3B	828,540,070	0.10	Angle	8.60	−0.18	0.07
Leaf	RAC875_c26353_719	5A	552,784,446	0.16	AUDPC_GDD	11.16	2100.9	0.01
Leaf	AX-158542533	5A	552,843,755	0.15	GDD50	7.05	−21.34	0.02
Leaf	TG0128	5A	552,863,415	0.16	maxVar	5.42	3.69	0.00
Leaf	Kukri_rep_c72553_368	5B	588,418,161	0.15	AUDPC_GDD	14.37	−2625.16	0.14
Leaf	AX-110574793	5B	592,019,656	0.16	Angle	9.34	−0.18	0.11
Leaf	Excalibur_c64119_345	6B	12,380,969	0.17	Angle	6.44	0.13	0.02
Leaf	AX-158590198	7A	570,120,295	0.28	AUDPC_GDD	7.81	−1237.71	0.09
Leaf	Kukri_c42807_473	7A	603,303,689	0.35	Angle	7.21	−0.12	0.02
Leaf	wsnp_Ra_c39394_47110214	7A	695,829,528	0.26	Angle	12.25	−0.26	0.03

Abbreviation: SNP, single nucleotide polymorphism

with no shared loci between diseases. These associations mapped to 10 chromosomes: Chromosomes 1A, 2B, 3A, 3B, 4B, 5A, 5B, and 7A for yellow rust, and chromosomes 2A, 2B, 3B, 5A, 5B, 6B, and 7A for leaf rust (Table 2; Figure 5). For yellow rust, five genomic regions consistently associate across most or all disease metrics. These regions are located at positions 538 Mbp on chromosome 1A, 767 Mbp on 2B, 754 Mbp on 3B, 684 Mbp on 5B, and 709 Mbp on 7A.

Furthermore, the `AUDPC_GDD` metric identifies nine unique associations with yellow rust not detected by other metrics. These include loci at positions 602 Mbp on chromosome 3A; 5 Mbp, 72 Mbp, and 243 Mbp on chromosome 3B; 650 Mbp

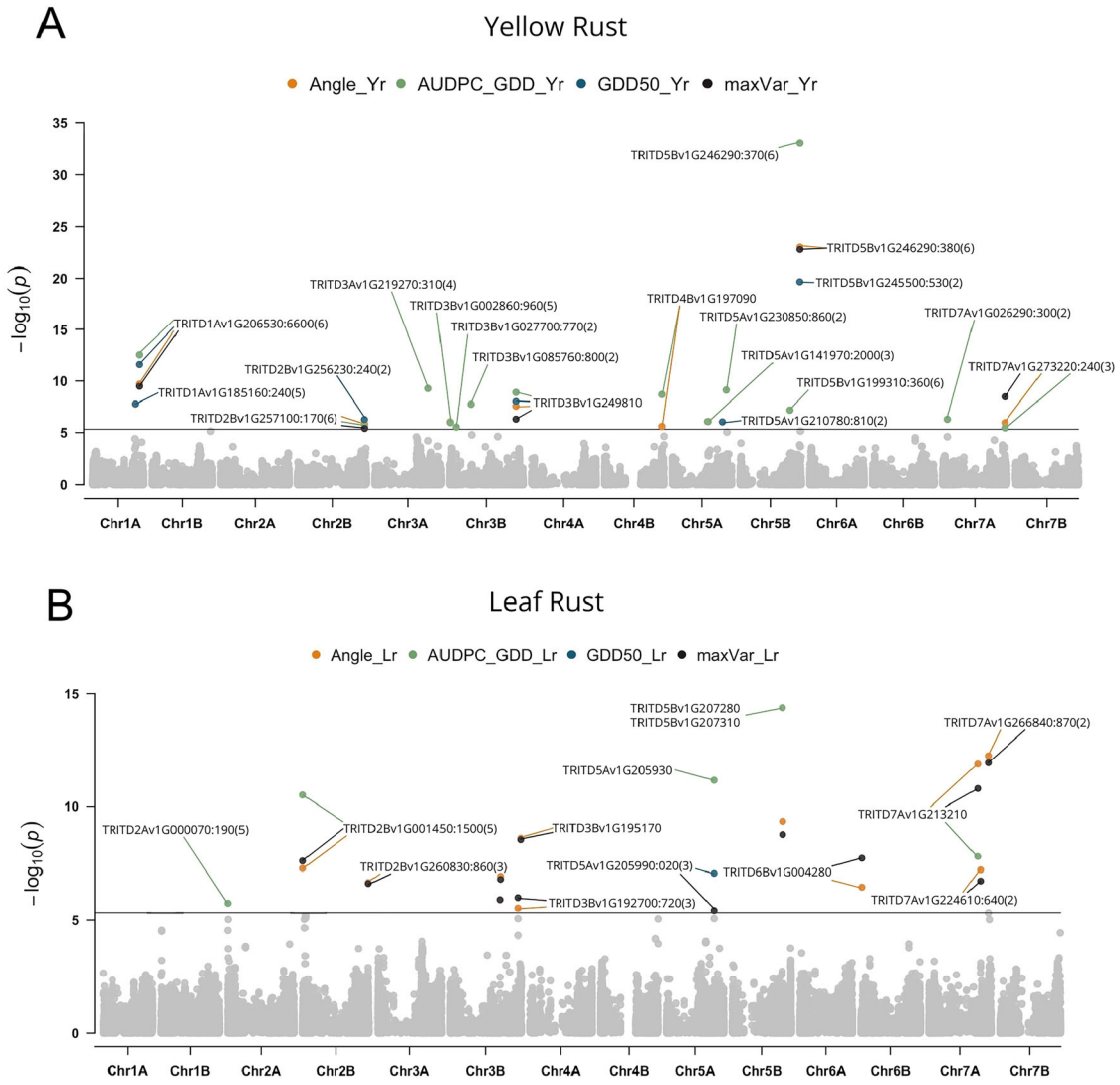

FIGURE 5 Manhattan plots for four disease metrics across two panels: (A) for yellow rust and (B) for leaf rust. Each point represents the $-\log_{10}$ of the *p*-value for a single nucleotide polymorphism (SNP) plotted against its genomic position. The dark horizontal line indicates the significance threshold (*p*-value < 0.05 after Bonferroni correction, corresponding to logarithm of the odds [LOD] = 5.32). Points above this threshold are colored based on the disease metric they are associated with. Candidate genes detected near each hit are named in the plot pointing to its associated hit.

on chromosome 4B; 398 Mbp and 607 Mbp on chromosome 5A; 568 Mbp on chromosome 5B; and 52 Mbp on chromosome 7A. Two of these associations are also detected by the `Angle` metric, with one of these additionally identified by the `maxVar` metric. Overall, `AUDPC_GDD` detects the highest number of associations, capturing nearly all associations identified by other metrics.

For leaf rust, the `Angle` and `maxVar` metrics identify the highest number of associations and share considerable overlap. Specifically, shared associations occur at positions 2 Mbp and 776 Mbp on chromosome 2B; 588 Mbp and 595 Mbp on chromosome 3B; 12 Mbp on chromosome 6B; and 570 Mbp, 603 Mbp, and 695 Mbp on chromosome 7A. In contrast, the `GDD50` metric identifies only a single association.

The `AUDPC_GDD` metric detects three associations shared by `Angle` and `maxVar` metrics, as well as an additional unique association at 0.2 Mbp on chromosome 2A. Additionally, all metrics except `Angle` identify a significant association at 552 Mbp on chromosome 5A with different SNPs.

Figure 6 presents *Q*–*Q* plots for all traits, illustrating deviations from the null hypothesis of no association. These plots highlight potential genomic regions linked to disease metrics and confirm the quality of the GWAS analysis.

3.3 | Genomic prediction accuracy and model comparisons

We evaluated the impact of including GWAS hits as fixed effects on genomic prediction accuracy by comparing the performance of three models (GBLUP, BayesB, and RKHS) with and without these significant markers (Figure 7).

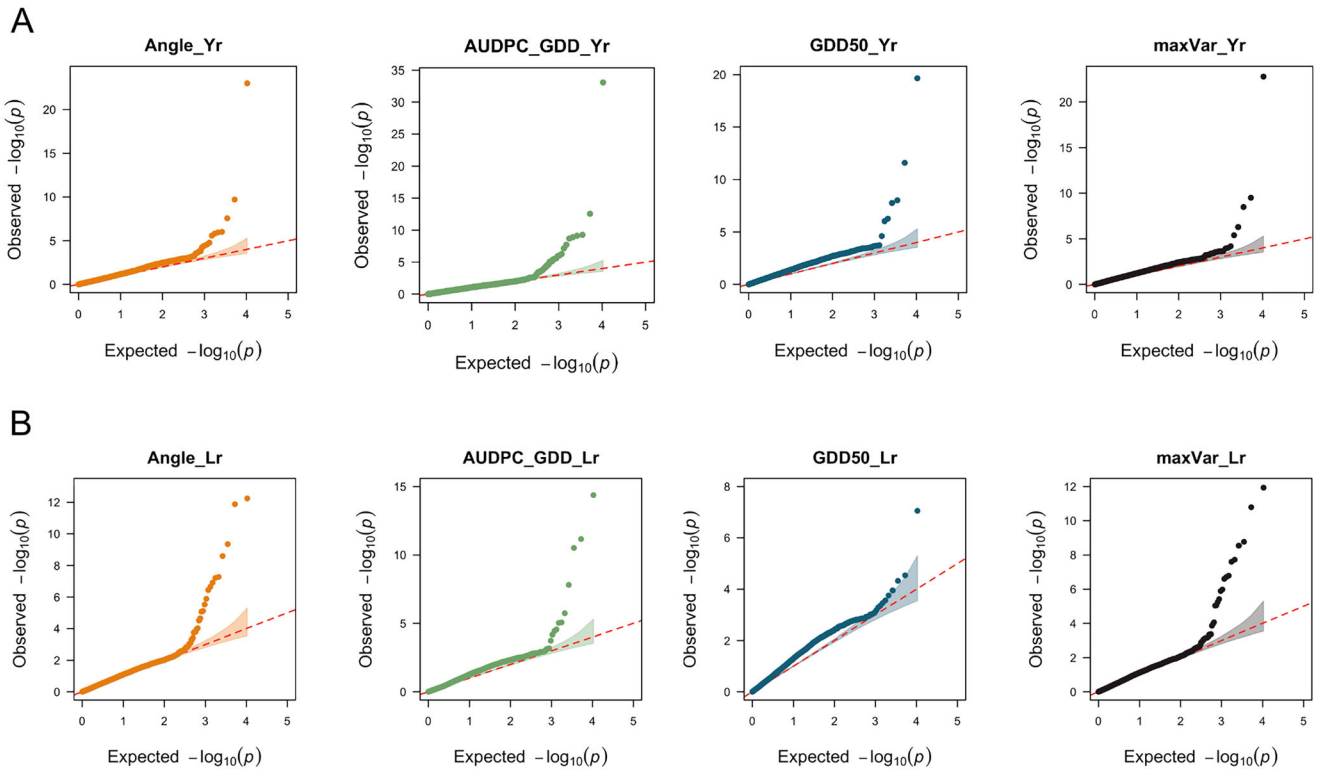

FIGURE 6 Quantile-Quantile (Q–Q) plots for four disease metrics, divided into two panels: (A) for yellow rust and (B) for leaf rust. Each point represents the $-\log_{10}$ of the observed p-value for an SNP plotted against its expected value under the null hypothesis of no association. The plots help assess the deviation of observed p-values from the expected distribution, indicating potential associations.

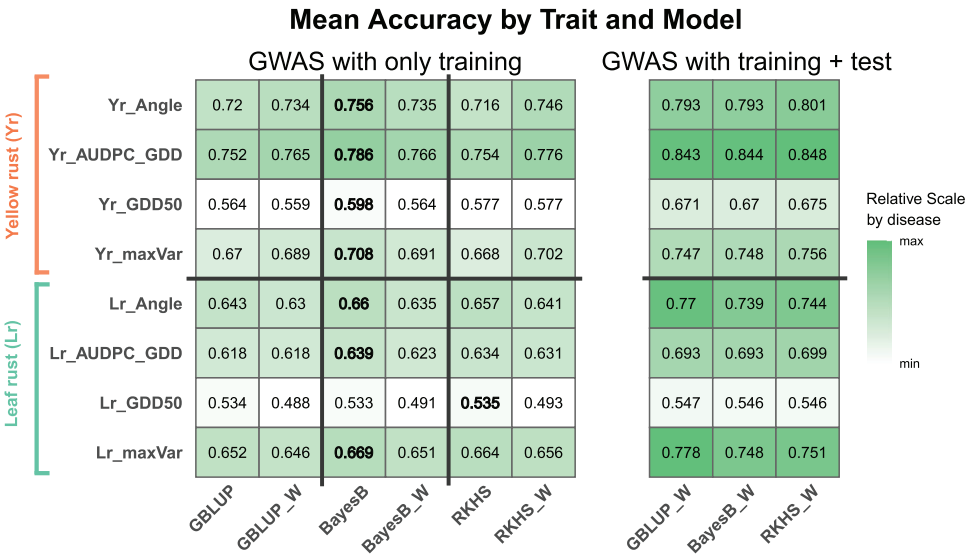

FIGURE 7 Summary of assay accuracies: Mean accuracy across 60 assay repetitions, comparing the performance of the tested models under three conditions: (1) the standard model assessment without fixed effects, (2) when significant genome-wide association study (GWAS) hits from the training population are included as fixed effects (_W, "Weighted"), and (3) when significant GWAS hits from the entire population (training and test) are included as fixed effects (separate table) as an example of data leakage. Accuracy values are color-coded from white (lowest) to green (highest), with coding distinct for each disease. The highest accuracy achieved on each metric, excluding the data leakage assessment, is highlighted in bold. Lr, leaf rust; Yr, yellow rust.

Since GS models should not incorporate phenotypic data from the test set, we identified GWAS hits exclusively from each training set, as previously mentioned (Section 2.7). To accomplish this, we performed a GWAS separately on each of the training sets of the 60 repetitions generated during cross-validation, referring to this scenario as the *Weighted* ("_W") approach.

For comparison, we repeated the analysis using GWAS hits previously reported in Section 3.2, which were identified using the complete dataset, thus introducing data leakage from the test population. Results from this positive control scenario are presented separately in Figure 7 (right).

As expected, incorporating GWAS hits identified from the entire population significantly improves prediction accuracy across all metrics and models, confirming that our positive control functions correctly.

In contrast, when incorporating GWAS hits identified exclusively from the training sets, prediction accuracy generally does not improve and sometimes decreases slightly. The only notable exception occurs for yellow rust metrics using the RKHS model, although these improvements are not statistically significant (Figure S3).

Among all tested models, BayesB without GWAS hits achieves the highest overall prediction accuracy, though its performance is also not statistically different from BayesB with GWAS hits or the RKHS model (Figure S3).

3.4 | Candidate genes and functional annotation analyses

We identified 42 high-confidence candidate genes underlying yellow rust resistance across eight genomic regions (chromosomes 1A, 2B, 3A, 3B, 4B, 5A, 5B, and 7A; Table S1). These include multiple serine/threonine kinases and leucine-rich repeat (LRR) proteins, key components of plant immune signaling, as well as enzymes involved in secondary metabolism (e.g., UDP-glycosyltransferases and 4-coumarate-CoA ligase) and stress-responsive factors such as LEA-2 proteins and superoxide dismutases. GO enrichment analysis highlighted "protein phosphorylation," "oxidation-reduction process," and related defense pathways (Figure 8A,B). Within-trait correlations among yellow rust metrics (`AUDPC_GDD`, `Angle`, `maxVar`) were strong, whereas cross-disease correlations were negligible (Figure 8C).

For leaf rust, we mapped five marker trait associations (MTAs) to seven chromosomes (2A, 2B, 3B, 5A, 5B, 6B, and 7A), from which 28 candidate genes were selected (Table S1). Prominent among these are NB-ARC (nucleotide binding–Apaf-1, R proteins, and CED-4) and LRR-type resistance proteins, RING (really interesting new gene)-type E3 ubiquitin ligases, and serine/threonine phosphatases involved in protein turnover, and hormone and ion-transport regulators such as ethylene receptors and potassium/proton antiporters. GO class distributions show a balance between biological process and molecular function categories (Figure 8D).

Together, these results suggest that both yellow and leaf rust resistance in this panel rely on a combination of canonical immune receptors, signaling kinases, and metabolic enzymes. The detailed correspondence between MTAs and candidate genes is provided in Table S1, and gene annotations are provided in Table S2.

4 | DISCUSSION

4.1 | Yellow and leaf rust MTAs revealed by GWAS

LD analysis indicated that the correlation between markers (r^2) decayed below 0.2 at an average physical distance of 12.5 Mbp. Based on this threshold, we assumed that GWAS associations located within 12.5 Mbp of known loci likely correspond to the same underlying genetic signal. To account for variability in recombination rates both across and within chromosomes, we adopted a conservative criterion: Only associations located more than 14 Mbp from any previously reported gene or QTL were considered potentially novel.

4.1.1 | Yellow rust disease

We identified two potentially novel signals for yellow rust resistance, both detected exclusively using the `AUDPC_GDD` metric. The first is located at 602.7 Mbp on chromosome 3A, approximately 15 Mbp away from the nearest previously reported association (Sharma et al., 2025), suggesting it may represent a distinct locus. The second novel signal was found at 243.4 Mbp on chromosome 3B, 23 Mbp away from the nearest reported signal (Sharma et al., 2025).

Other MTAs coincide with known genomic regions or resistance genes. On chromosome 1A, signals at 492 Mbp and 538 Mbp align with signals of multiple earlier studies (Bokore et al., 2017; Bai et al., 2022; Mahmood et al., 2022). Chromosome 2B shows a strong association near 767 Mbp, consistently reported in the literature (Christiansen et al., 2006; Tong et al., 2024). On chromosome 3B, MTAs at 3 Mbp and 5.5 Mbp are close to *Yr30* and *Yr57* (positioned at 1.17 and 2.51 Mbp) (J. Kaur et al., 2009; Randhawa et al., 2015), while the MTA at 72 Mbp matches previously reported loci (Hao et al., 2011). Similarly, the MTA at 754.5 Mbp (identified by all metrics) aligns closely with *Yr82* (757 Mbp) (Pakeerathan et al., 2019) and nearby associations (U. K. Bansal et al., 2013; P. Zhang, Yan, et al., 2021).

We detected one MTA on chromosome 4B that matches reported signals (Bokore et al., 2017; Cheng et al., 2022).

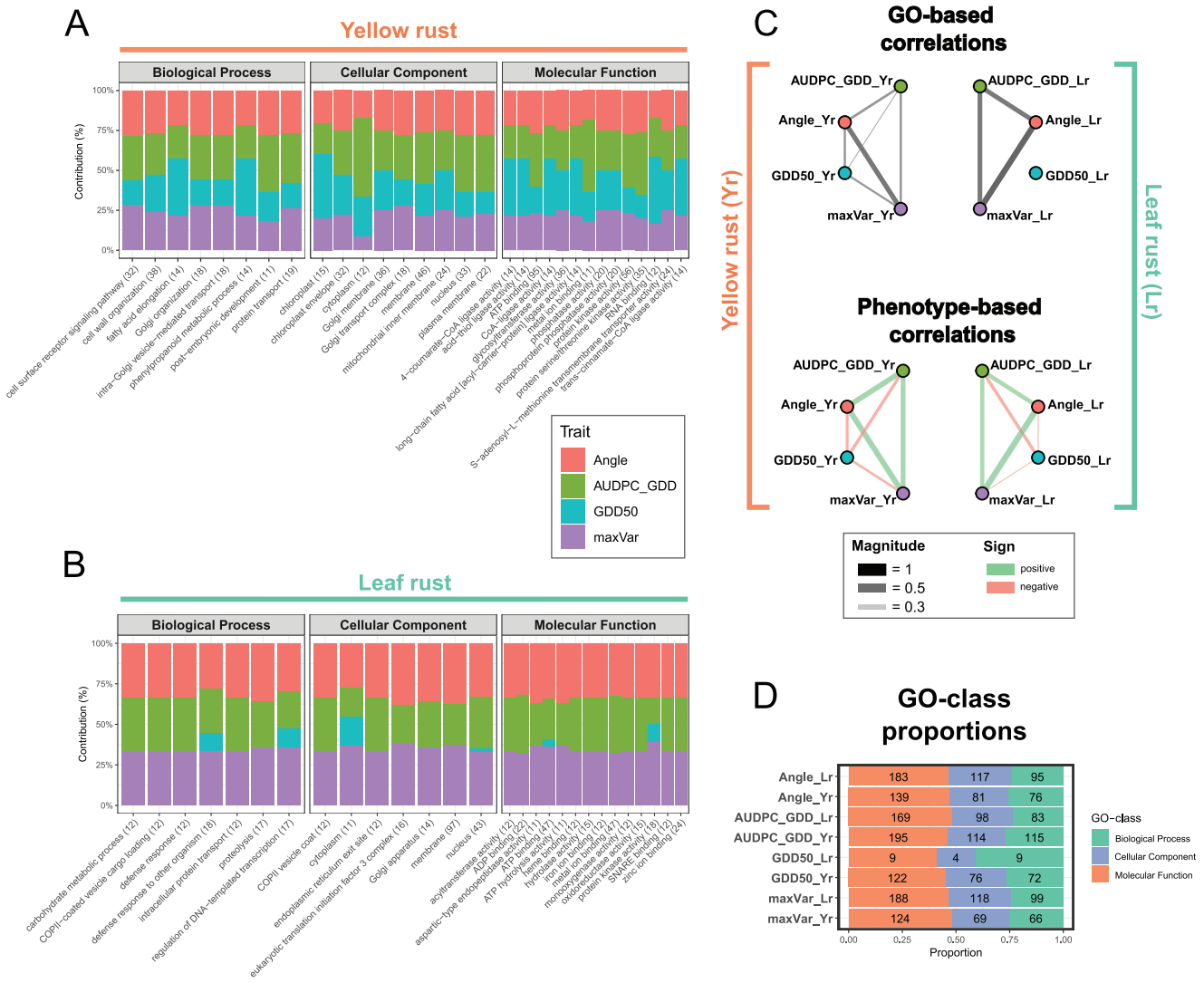

FIGURE 8 Gene ontology (GO) analysis of candidate genes. Stacked bar plots displaying the top 10 GO terms identified for (A) yellow rust and (B) leaf rust. Bars represent the percentage contribution of each disease severity metric (`Angle`, `AUDPC_GDD`, `GDD50`, and `maxVar`) to each GO term, categorized into biological process, cellular component, and molecular function. (C) GO-based and phenotype-based correlations among the four metrics for both diseases. Edge thickness indicates correlation magnitude, while color denotes positive (green) or negative (red) correlations. (D) Proportions of GO-class annotations for candidate genes detected by each metric.

On chromosome 5A, one MTA at 398.1 Mbp is 6 Mbp away from a seedling-stage MTA found only in one study in bread wheat (Sharma et al., 2025), suggesting it could have the same underlying genetic factor but now detected in the adult plant stage. An MTA at 563 Mbp on this same chromosome is on the same linkage block as the known *YrU1* gene (H. Wang et al., 2020) and another published MTA (X. Chen, 2020), while a nearby signal at 607.9 Mbp was also detected on the same linkage block in another study (Farzand et al., 2022). Chromosome 5B has two distinct MTA clusters, each on the same linkage blocks as earlier studies (Aoun et al., 2021; Bokore et al., 2021; Calvo-Salazar et al., 2015; Cheng et al., 2022; Mahmood et al., 2022; Zou et al., 2017). Lastly, two MTAs emerged on chromosome 7A: the first, found only by `AUDPC_GDD`, aligns closely with Mahmood et al. (2022), and the second at 709 Mbp matches multiple prior reports (Mahmood et al., 2022; P. Zhang, Yan, et al., 2021).

4.1.2 | Leaf rust disease

Our GWAS also revealed two potentially novel MTAs for leaf rust. The first one on chromosome 5A is detected by all metrics except `Angle` at 552.8 Mbp, which is over 15 Mbp away from known associations (Bokore et al., 2020; P. Zhang, Yan, et al., 2021) on the same chromosome. And the second potentially novel locus on chromosome 7A is located at 570 Mbp, about 19 Mbp away from a previously reported signal (Lakkakula et al., 2025).

Several other detected MTAs are on the same linkage block as other established loci or genes. On chromosome 2A, the MTA at 0.2 Mbp is very close to the *Lr65* and *Lr17a* genes (on positions 1.64 and 5.88 Mbp) (Bremenkamp-Barrett et al., 2008; Q. Zhang, Wei, et al., 2021), suggesting one or both of them are probably the underlying factor behind the signal. Additional studies (Bokore et al., 2020; Talebi et al., 2023) have found signals in the same region, probably due to the same reason. On chromosome 2B, an MTA at 2.5 Mbp is on the same linkage block as *Lr16* (at position 5.8 Mbp) (McCartney et al., 2005) and a previously known MTA (Tsilo et al., 2014). While another MTA on this same chromosome (776 Mbp) is on the same linkage block as other signals reported in two previous studies (S. Kaur et al., 2023; Rosa et al., 2019). Chromosome 3B harbors MTAs at 589, 595, 795, and 828 Mbp, all of them landing on the same linkage block as other published loci (Bokore et al., 2024; Chu et al., 2009; S. Kaur et al., 2023; Talebi et al., 2023; P. Zhang et al., 2019).

On chromosome 5B, an MTA at 588 Mbp is on the same linkage block as *Lr18* (576.3 Mbp) (Sadeghabad et al., 2017), while a nearby MTA (592 Mbp) can also be linked to other published associations (Chu et al., 2009; S. Kaur et al., 2023). The chromosome 6B MTA at 12.4 Mbp aligns with earlier findings (Kthiri et al., 2019; S. Kaur et al., 2023) but is too distant from *Lr53* or *Lr61* (Dadkhodaie et al., 2010; Herrera-Foessel et al., 2008) to indicate direct causality. Lastly, on chromosome 7A, MTAs at 603 Mbp and 695 Mbp land near signals reported on multiple prior studies (Bokore et al., 2020; Genievskaya et al., 2020; Mahmood et al., 2022; P. Zhang, Yan, et al., 2021).

4.2 | Optimizing phenotyping metrics for rust resistance

Our analysis revealed different optimal metrics depending on the rust disease. For yellow rust, `AUDPC_GDD` identified the most MTAs in GWAS and consistently achieved the highest mean predictive accuracy across GS models. Although its advantage over `Angle` was not statistically significant (Figure S3), `AUDPC_GDD` routinely outperformed other metrics, likely reflecting its elevated heritability and CV (Figure 3), which aids in detecting genomic effects.

By contrast, for leaf rust, `maxVar` was marginally superior, closely followed by `Angle`. Both metrics identified broadly overlapping MTAs, with `maxVar` revealing one additional locus on chromosome 5A. Although `maxVar` achieved a slightly higher mean accuracy than `Angle`, neither difference was statistically significant (Figure S3). In contrast, `AUDPC_GDD` consistently showed lower mean accuracy for leaf rust, albeit not at a significant level. The advantage of `Angle` and `maxVar` for leaf rust likely reflects their relatively higher heritability in this context (Figure 3).

No single metric excelled across both diseases. The weaker performance of `GDD50` likely arises from incomplete infection progress, as many lines did not reach 50% disease severity (Figure 1C). This underscores how the best metric may depend on phenotyping logistics and disease progression patterns.

Each metric offers distinct benefits. `GDD50` highlights latency-period resistance (Das et al., 1993), relying on precise timing to capture 50% infection. `Angle` requires only one assessment (optimally just at disease maturity), making it resource-efficient but vulnerable to slight timing errors. `maxVar` targets the time of greatest phenotypic variance, potentially requiring just one well-chosen measurement only if historical data are available. Meanwhile, `AUDPC_GDD` integrates the entire epidemic trajectory, serving as a comprehensive but more labor-intensive measure.

Phenology differences across genotypes and environments can complicate selecting an optimal sampling window, but reduced genetic diversity in breeding programs may ease this challenge. In practice, breeders can balance resource availability with the specific component of rust resistance they aim to improve. When measurements are limited, `Angle` or `GDD50` can be effective if disease milestones are predictable; with multiple assessments in hand, `maxVar` may enhance discrimination; and if comprehensive sampling is feasible, `AUDPC_GDD` remains robust. Testing multiple metrics and comparing their predictive accuracy or heritability can guide the choice of phenotyping strategy for targeted rust resistance breeding.

4.3 | GS strategies for rust resistance

Having established that the best disease-scoring metric depends on both phenotyping resources and the population structure, we next evaluated how effectively these metrics feed into GS frameworks for rust resistance. Specifically, we investigated whether incorporating GWAS-identified major-effect loci as fixed effects could enhance prediction accuracy.

Although modeling known major loci often appears promising (Bernardo, 2014; Rutkoski et al., 2014), our results did not show improvements (Figure 7; Figure S3). In fact, incorporating GWAS-derived fixed effects slightly, but not significantly, reduced accuracy across GS models and metrics. We hypothesize that trying to estimate the effect of numerous large-effect loci may impede the estimation of background low-effect loci (Bernardo, 2001, 2014). Our positive-control analysis (Figure 7) confirmed that these models can leverage fixed effects effectively, but the observed gains likely stemmed from data leakage from the validation set. Such findings reinforce the need for rigorous validation of any modeling approach similar to this one, given potential confounding from test-set information.

Despite these challenges, Bayesian methods, in particular BayesB, which assumes a sparse genetic architecture (few large effects, many small effects; De Los Campos et al., 2010), consistently achieved the highest average predictive accuracy. Although not a statistically significant edge, this tendency suggests BayesB may be slightly better suited to the genetic basis of rust resistance in our population (Bouvet et al., 2021; D. Kumar et al., 2020).

4.4 | Candidate gene identification and functional insights

Among the 36 GWAS-detected MTAs, seven (3B, 3 and 5.5 Mbp; 3B, 3 and 5.5 Mbp; 3B, 754.5 Mbp; 5A, 607 Mbp; 2B, 2.5 Mbp; 2A, 0.2 Mbp; 5B, 588 Mbp; 2A, 0.2 Mbp) are near established rust resistance genes (*Yr30*, *Yr57*, *Yr82*, *YrU1*, *Lr16*, *Lr17a*, *Lr18*, and *Lr65*; Section 4.1), suggesting they likely tag causal variants. The remaining MTAs were investigated for candidate genes (Section 3.4), revealing several harboring F-box domains (e.g., 776 Mbp on chromosome 2B and 72 Mbp on chromosome 3B), which have been implicated in fungal resistance (Gidhi et al., 2022; van den Burg et al., 2008). We also found serine/threonine kinases near MTAs at 588.7 Mbp (3B), 602.7 Mbp (3A), and 709 Mbp (7A), mirroring critical roles in defense signaling (e.g., *Yr15*) (Anderson et al., 2006; Klymiuk et al., 2018; Tang et al., 1999).

A notable leaf rust MTA on chromosome 5A (552.8 Mbp) is close to an NB-ARC domain-containing gene, a hallmark of NLR-type resistance (e.g., *Yr10*) (Prasad et al., 2020; Wu et al., 2025; Yildirim-Ersoy et al., 2011). Two yellow rust MTAs on chromosome 1A also lie near NLR genes, reinforcing their candidacy. An additional EF-hand protein in this locus has been tied to defense against diverse stresses (A. Kaur et al., 2022). On chromosome 7A, an MTA links to a sucrose-phosphate synthase gene, potentially linking sugar metabolism and rust susceptibility (Spanic et al., 2023). Another pair of MTAs at 767.7 Mbp on chromosome 2B and 602.7 Mbp on chromosome 3A associate with allantoinase and uricase genes, implicated in rust–host interactions (Montalbini, 1992, 1995).

MTAs on chromosomes 3A and 3B lie near LEA (late embryogenesis abundant) domain-2 proteins, putatively involved in desiccation tolerance and defense (Magwanga et al., 2018) (Table S1). Although unproven in rust, their recurring presence suggests a novel mechanism for further exploration. On chromosome 5A (607 Mbp), a WH2 (WASP homology)-domain gene involved in actin nucleation (Arp2/3 complex) may relate to yellow rust resistance (Guo et al., 2022; Qi, 2017). Additionally, MTAs on chromosome 5B (602 Mbp) lie near a RIN4 (RPM1-interacting protein 4)-domain protein, shown to interact with barley *RPG1* for stem rust resistance (Gill et al., 2012). Another candidate at 52 Mbp on chromosome 7A encodes a superoxide dismutase, reported to increase in wheat under stripe rust (Asthir et al., 2010), and at 709 Mbp, an MTA maps near a Mediator complex subunit, *Med15*, implicated in stem rust defense (Hiebert et al., 2020).

5 | CONCLUSION

Our GWAS in Canadian durum wheat confirmed associations near established resistance genes (e.g., *Yr30, Yr57, Yr82, YrU1, Lr16, Lr17, Lr18*, and *Lr65*) and revealed novel MTAs linked to diverse candidate genes. We detect two novel MTAs on chromosomes 3A and 3B for yellow rust, flanked by genes for a serine/threonine kinase and a uricase enzyme. For leaf rust, we identified additional MTAs on chromosomes 5A and 7A, including regions harboring NB-ARC domain-containing proteins and serine/threonine kinases. These findings underscore the genetic diversity underpinning rust resistance, where optimal phenotyping metrics (`AUDPC_GDD` for yellow rust and `maxVar` for leaf rust) and the BayesB model emerged as particularly effective for enhancing breeding. Incorporating GWAS hits as fixed effects did not enhance GS prediction accuracies, underscoring the complex genetic basis of rust resistance. These findings provide valuable targets for functional validation and practical guidance for developing more durable, rust-resistant durum wheat cultivars.

AUTHOR CONTRIBUTIONS

Juan Menor de Gaspar: Conceptualization; Data curation; Formal analysis; Investigation; Methodology; Software; Visualization; Writing–original draft. **Alejandro Domínguez Rondón**: Methodology; Software; Visualization. **Julián García-Abadillo**: Conceptualization; Data curation; Formal analysis; Investigation; Software; Supervision; Visualization; Writing–review & editing. **Ron Knox**: Conceptualization; Resources; Supervision; Writing–review & editing. **Firdissa E. Bokore**: Resources; Writing–review & editing. **Kerry Boyle**: Resources; Supervision. **Karim Ammar**: Resources. **Julio Huerta-Espino**: Data curation; Resources. **Samia Berraies**: Resources. **Brad Meyer**: Resources. **Wentao Zhang**: Resources. **Richard D. Cuthbert**: Funding acquisition; Resources; Writing–review & editing. **Fobert Pierre**: Conceptualization; Resources; Supervision. **Ruan Yuefeng**: Funding acquisition; Project administration; Resources; Writing–review & editing. **Julio Isidro y Sánchez**: Conceptualization; Data curation; Funding acquisition; Project administration; Supervision; Writing–original draft.

ACKNOWLEDGMENTS

The authors would like to thank all researchers and technicians at the AAFC Swift Current Research and Development Centre (SCRDC) in Canada for their valuable contributions to the breeding program. Phenotyping and genotyping supports were provided by the Government of Saskatchewan

Agriculture Development Fund (Project Number 20130015), the Saskatchewan Wheat Development Commission (Project number 171025-63), Agriculture and Agri-Food Canada, and through the Canadian National Wheat Cluster program and the Canadian Wheat Research Coalition. We also acknowledge the Wheat Improvement Flagship Program, which is the National Research Council of Canada's contribution to the Canadian Wheat Alliance. Julio Isidro y Sánchez, Juan Menor de Gaspar, and Alejandro Domínguez Rondón were supported by Grant PID2021-123718OB-I00 funded by MCIN/AEI/10.13039/501 494 100 011 033 and by ERDF A way of making Europe, CEX2020-000999-S.

CONFLICT OF INTEREST STATEMENT

The authors declare no conflicts of interest.

DATA AVAILABILITY STATEMENT

The datasets analyzed and generated during the current study are available in our GitHub repository at https://github.com/Brad-Meyer/AAFC-SCRDC_Publications.

ORCID

Juan Menor de Gaspar https://orcid.org/0009-0002-6459-7785
Julián García-Abadillo https://orcid.org/0000-0002-4672-8908
Wentao Zhang https://orcid.org/0000-0003-4301-1597
Julio Isidro y Sánchez https://orcid.org/0000-0002-9044-3221

REFERENCES

Akdemir, D., Knox, R., & Isidro y Sánchez, J. (2020). Combining partially overlapping multi-omics data in databases using relationship matrices. *Frontiers in Plant Science*, *11*, 947. https://doi.org/10.3389/fpls.2020.00947

Alemu, S. K., Huluka, A. B., Tesfaye, K., Haileselassie, T., & Uauy, C. (2021). Genome-wide association mapping identifies yellow rust resistance loci in Ethiopian durum wheat germplasm. *PLOS ONE*, *16*(5), e0243675. https://doi.org/10.1371/journal.pone.0243675

Anderson, J. C., Pascuzzi, P. E., Xiao, F., Sessa, G., & Martin, G. B. (2006). Host-mediated phosphorylation of type iii effector AvrPto promotes *Pseudomonas* virulence and avirulence in tomato. *The Plant Cell*, *18*(2), 502–514. https://doi.org/10.1105/tpc.105.036590

Aoun, M., Breiland, M., Kathryn Turner, M., Loladze, A., Chao, S., Xu, S. S., Ammar, K., Anderson, J. A., Kolmer, J. A., & Acevedo, M. (2016). Genome-wide association mapping of leaf rust response in a durum wheat worldwide germplasm collection. *The Plant Genome*, *9*(3). https://doi.org/10.3835/plantgenome2016.01.0008

Aoun, M., Rouse, M. N., Kolmer, J. A., Kumar, A., & Elias, E. M. (2021). Genome-wide association studies reveal all-stage rust resistance loci in elite durum wheat genotypes. *Frontiers in Plant Science*, *12*, 640739. https://doi.org/10.3389/fpls.2021.640739

Ashburner, M., Ball, C. A., Blake, J. A., Botstein, D., Butler, H., Cherry, J. M., Davis, A. P., Dolinski, K., Dwight, S. S., Eppig, J. T., Harris, M. A., Hill, D. P., Issel-Tarver, L., Kasarskis, A., Lewis, S., Matese, J. C., Richardson, J. E., Ringwald, M., Rubin, G. M., & Sherlock, G. (2000). Gene ontology: Tool for the unification of biology. *Nature Genetics*, *25*(1), 25–29. https://doi.org/10.1038/75556

Asthir, B., Koundal, A., Bains, N. S., & Mann, S. K. (2010). Stimulation of antioxidative enzymes and polyamines during stripe rust disease of wheat. *Biologia Plantarum*, *54*(2), 329–333. https://doi.org/10.1007/s10535-010-0057-4

Bai, B., Li, Z., Wang, H., Du, X., Wu, L., Du, J., & Lan, C. (2022). Genetic analysis of adult plant resistance to stripe rust in common wheat cultivar "pascal". *Frontiers in Plant Science*, *13*, 918437. https://doi.org/10.3389/fpls.2022.918437

Bansal, M., Kaur, S., Dhaliwal, H. S., Bains, N. S., Bariana, H. S., Chhuneja, P., & Bansal, U. K. (2016). Mapping of *Aegilops umbellulata*-derived leaf rust and stripe rust resistance loci in wheat. *Plant Pathology*, *66*(1), 38–44. https://doi.org/10.1111/ppa.12549

Bansal, U. K., Kazi, A. G., Singh, B., Hare, R. A., & Bariana, H. S. (2013). Mapping of durable stripe rust resistance in a durum wheat cultivar wollaroi. *Molecular Breeding*, *33*(1), 51–59. https://doi.org/10.1007/s11032-013-9933-x

Bates, D., Mächler, M., Bolker, B., & Walker, S. (2015). Fitting linear mixed-effects models usinglme4. *Journal of Statistical Software*, *67*(1), 1–48. https://doi.org/10.18637/jss.v067.i01

Bernardo, R. (2001). What if we knew all the genes for a quantitative trait in hybrid crops?. *Crop Science*, *41*(1), 1–4. https://doi.org/10.2135/cropsci2001.4111

Bernardo, R. (2014). Genomewide selection when major genes are known. *Crop Science*, *54*(1), 68–75. https://doi.org/10.2135/cropsci2013.05.0315

Bokore, F. E., Boyle, K., Ruan, Y., McCartney, C. A., Hiebert, C. W., Knox, R. E., Pei, X., Reimer, E., Ammar, K., Zhang, W., Fobert, P., Cuthbert, R. D., Berraies, S., & McCallum, B. D. (2024). Mapping seedling and adult plant leaf rust resistance genes in the durum wheat cultivar strongfield and other *Triticum turgidum* lines. *Phytopathology*, *114*(11), 2401–2411. https://doi.org/10.1094/PHYTO-09-23-0348-R

Bokore, F. E., Cuthbert, R. D., Knox, R. E., Randhawa, H. S., Hiebert, C. W., DePauw, R. M., Singh, A. K., Singh, A., Sharpe, A. G., N'Diaye, A., Pozniak, C. J., McCartney, C., Ruan, Y., Berraies, S., Meyer, B., Munro, C., Hay, A., Ammar, K., Huerta-Espino, J., & Bhavani, S. (2017). Quantitative trait loci for resistance to stripe rust of wheat revealed using global field nurseries and opportunities for stacking resistance genes. *Theoretical and Applied Genetics*, *130*(12), 2617–2635. https://doi.org/10.1007/s00122-017-2980-7

Bokore, F. E., Knox, R. E., Cuthbert, R. D., Pozniak, C. J., McCallum, B. D., N'Diaye, A., DePauw, R. M., Campbell, H. L., Munro, C., Singh, A., Hiebert, C. W., McCartney, C. A., Sharpe, A. G., Singh, A. K., Spaner, D., Fowler, D. B., Ruan, Y., Berraies, S., & Meyer, B. (2020). Mapping quantitative trait loci associated with leaf rust resistance in five spring wheat populations using single nucleotide polymorphism markers. *PLOS ONE*, *15*(4), e0230855. https://doi.org/10.1371/journal.pone.0230855

Bokore, F. E., Ruan, Y., Mccartney, C., Knox, R. E., Pei, X., Aboukhaddour, R., Randhawa, H., Ammar, K., Meyer, B., Cuthbert, R. D., Berraies, S., Depauw, R., & Fobert, P. (2021). High density genetic mapping of stripe rust resistance in a 'strongfield'/'blackbird' durum wheat population. *Canadian Journal of Plant Pathology*, *43*(sup2), S242–S255. https://doi.org/10.1080/07060661.2021.1968036

Bouvet, L., Percival-Alwyn, L., Berry, S., Fenwick, P., Mantello, C. C., Sharma, R., Holdgate, S., Mackay, I. J., & Cockram, J. (2021). Wheat

genetic loci conferring resistance to stripe rust in the face of genetically diverse races of the fungus *Puccinia striiformis* f. sp. tritici. *Theoretical and Applied Genetics*, *135*(1), 301–319. https://doi.org/10.1007/s00122-021-03967-z

Bremenkamp-Barrett, B., Faris, J. D., & Fellers, J. P. (2008). Molecular mapping of the leaf rust resistance gene lr17a in wheat. *Crop Science*, *48*(3), 1124–1128. https://doi.org/10.2135/cropsci2007.07.0379

van den Burg, H. A., Tsitsigiannis, D. I., Rowland, O., Lo, J., Rallapalli, G., MacLean, D., Takken, F. L., & Jones, J. D. (2008). The f-box protein acre189/acif1 regulates cell death and defense responses activated during pathogen recognition in tobacco and tomato. *The Plant Cell*, *20*(3), 697–719. https://doi.org/10.1105/tpc.107.056978

Calvo-Salazar, V., Singh, R. P., Huerta-Espino, J., Cruz-Izquierdo, S., Lobato-Ortiz, R., Sandoval-Islas, S., Vargas-Hernández, M., German, S., Silva, P., Basnet, B. R., Lan, C. X., & Herrera-Foessel, S. A. (2015). Genetic analysis of resistance to leaf rust and yellow rust in spring wheat cultivar Kenya Kongoni. *Plant Disease*, *99*(8), 1153–1160. https://doi.org/10.1094/PDIS-07-14-0718-RE

Chen, W., Wellings, C., Chen, X., Kang, Z., & Liu, T. (2014). Wheat stripe (yellow) rust caused by *Puccinia striiformis* f. sp. tritici. *Molecular Plant Pathology*, *15*(5), 433–446. https://doi.org/10.1111/mpp.12116

Chen, X. (2020). Pathogens which threaten food security: *Puccinia striiformis*, the wheat stripe rust pathogen. *Food Security*, *12*(2), 239–251. https://doi.org/10.1007/s12571-020-01016-z

Cheng, B., Gao, X., Cao, N., Ding, Y., Chen, T., Zhou, Q., Gao, Y., Xin, Z., & Zhang, L. (2022). QTL mapping for adult plant resistance to wheat stripe rust in M96-5 × Guixie 3 wheat population. *Journal of Applied Genetics*, *63*(2), 265–279. https://doi.org/10.1007/s13353-022-00686-z

Christiansen, M. J., Feenstra, B., Skovgaard, I. M., & Andersen, S. B. (2006). Genetic analysis of resistance to yellow rust in hexaploid wheat using a mixture model for multiple crosses. *Theoretical and Applied Genetics*, *112*(4), 581–591. https://doi.org/10.1007/s00122-005-0128-7

Chu, C.-G., Friesen, T. L., Xu, S. S., Faris, J. D., & Kolmer, J. A. (2009). Identification of novel QTLs for seedling and adult plant leaf rust resistance in a wheat doubled haploid population. *Theoretical and Applied Genetics*, *119*(2), 263–269. https://doi.org/10.1007/s00122-009-1035-0

Crossa, J., Sánchez-Villeda, H., Sorrells, M., & Jannink, J. (2012). Genomic selection in wheat breeding using genotyping-by-sequencing. *The Plant Genome*, *5*(3). https://doi.org/10.3835/plantgenome2012.06.0006

Dadkhodaie, N. A., Karaoglou, H., Wellings, C. R., & Park, R. F. (2010). Mapping genes lr53 and yr35 on the short arm of chromosome 6b of common wheat with microsatellite markers and studies of their association with lr36. *Theoretical and Applied Genetics*, *122*(3), 479–487. https://doi.org/10.1007/s00122-010-1462-y

Das, M. K., Rajaram, S., Kronstad, W. E., Mundt, C. C., & Singh, R. P. (1993). Associations and genetics of three components of slow rusting in leaf rust of wheat. *Euphytica*, *68*(1–2), 99–109. https://doi.org/10.1007/BF00024159

De Los Campos, G., Gianola, D., Rosa, G. J. M., Weigel, K. A., & Crossa, J. (2010). Semi-parametric genomic-enabled prediction of genetic values using reproducing kernel Hilbert spaces methods. *Genetics Research*, *92*(4), 295–308. https://doi.org/10.1017/S0016672310000285

Desiderio, F., Guerra, D., Rubiales, D., Piarulli, L., Pasquini, M., Mastrangelo, A. M., Simeone, R., Blanco, A., Cattivelli, L., & Vale', G. (2014). Identification and mapping of quantitative trait loci for leaf rust resistance derived from a tetraploid wheat *Triticum dicoccum* accession. *Molecular Breeding*, *34*(4), 1659–1675. https://doi.org/10.1007/s11032-014-0186-0

Dong, Z., Hegarty, J. M., Zhang, J., Zhang, W., Chao, S., Chen, X., Zhou, Y., & Dubcovsky, J. (2017). Validation and characterization of a QTL for adult plant resistance to stripe rust on wheat chromosome arm 6BS (Yr78). *Theoretical and Applied Genetics*, *130*(10), 2127–2137. https://doi.org/10.1007/s00122-017-2946-9

Dubin, H., & Rajaram, S. (1996). Breeding disease-resistant wheats for tropical highlands and lowlands. *Annual Review of Phytopathology*, *34*(1), 503–526. https://doi.org/10.1146/annurev.phyto.34.1.503

Endelman, J. B. (2011). Ridge regression and other kernels for genomic selection with r package rrblup. *The Plant Genome*, *4*(3), 250–255. https://doi.org/10.3835/plantgenome2011.08.0024

Farzand, M., Dhariwal, R., Hiebert, C. W., Spaner, D., & Randhawa, H. S. (2022). QTL mapping for adult plant field resistance to stripe rust in the AAC Cameron/P2711 spring wheat population. *Crop Science*, *62*(3), 1088–1106. https://doi.org/10.1002/csc2.20741

Figlan, S., Ntushelo, K., Mwadzingeni, L., Terefe, T., Tsilo, T. J., & Shimelis, H. (2020). Breeding wheat for durable leaf rust resistance in southern Africa: Variability, distribution, current control strategies, challenges and future prospects. *Frontiers in Plant Science*, *11*, 549. https://doi.org/10.3389/fpls.2020.00549

García-Abadillo, J., Barba, P., Carvalho, T., Sosa-Zuñiga, V., Lozano, R., Carvalho, H. F., Garcia-Rojas, M., Salazar, E., & y Sánchez, J. I. (2024). Dissecting the complex genetic basis of pre- and post-harvest traits in *Vitis vinifera* L. using genome-wide association studies. *Horticulture Research*, *11*(2), uhad283. https://doi.org/10.1093/hr/uhad283

Garcia-Abadillo, J., Morales, L., Buerstmayr, H., Michel, S., Lillemo, M., Holzapfel, J., Hartl, L., Akdemir, D., Carvalho, H. F., & Isidro-Sánchez, J. (2023). Alternative scoring methods of fusarium head blight resistance for genomic assisted breeding. *Frontiers in Plant Science*, *13*, 1057914. https://doi.org/10.3389/fpls.2022.1057914

Genievskaya, Y., Abugalieva, S., Rsaliyev, A., Yskakova, G., & Turuspekov, Y. (2020). QTL mapping for seedling and adult plant resistance to leaf and stem rusts in Pamyati Azieva × Paragon mapping population of bread wheat. *Agronomy*, *10*(9), 1285. https://doi.org/10.3390/agronomy10091285

Gidhi, A., Mohapatra, A., Fatima, M., Jha, S. K., Kumar, M., & Mukhopadhyay, K. (2022). Insights of auxin signaling f-box genes in wheat (*Triticum aestivum* L.) and their dynamic expression during the leaf rust infection. *Protoplasma*, *260*(3), 723–739. https://doi.org/10.1007/s00709-022-01808-4

Gill, U., Nirmala, J., Brueggeman, R., & Kleinhofs, A. (2012). Identification, characterization and putative function of HvRin4, a barley homolog of *Arabidopsis* Rin4. *Physiological and Molecular Plant Pathology*, *80*, 41–49. https://doi.org/10.1016/j.pmpp.2012.08.002

Giovanny, C.-P. (2016). Genome assisted prediction of quantitative traits using the r package sommer. *PLoS ONE*, *11*, 1–15.

Guo, J., Peng, H., Qi, T., Xu, S., Islam, M. A., Day, B., Ma, Q., Kang, Z., & Guo, J. (2022). Taarpc5 is required for wheat defense signaling in response to infection by the stripe rust fungus. *The Crop Journal*, *10*(1), 88–97. https://doi.org/10.1016/j.cj.2021.01.009

Hao, Y., Chen, Z., Wang, Y., Bland, D., Buck, J., Brown-Guedira, G., & Johnson, J. (2011). Characterization of a major QTL for adult plant resistance to stripe rust in US soft red winter wheat. *Theoretical and Applied Genetics*, *123*(8), 1401–1411. https://doi.org/10.1007/s00122-011-1675-8

Heffner, E. L., Lorenz, A. J., Jannink, J., & Sorrells, M. E. (2010). Plant breeding with genomic selection: Gain per unit time and cost. *Crop Science*, *50*(5), 1681–1690. https://doi.org/10.2135/cropsci2009.11.0662

Herrera-Foessel, S. A., Singh, R. P., Huerta-Espino, J., William, H. M., Djurle, A., & Yuen, J. (2008). Molecular mapping of a leaf rust resistance gene on the short arm of chromosome 6b of durum wheat. *Plant Disease*, *92*(12), 1650–1654. https://doi.org/10.1094/PDIS-92-12-1650

Herrera-Foessel, S. A., Singh, R. P., Huerta-Espino, J., William, M., Rosewarne, G., Djurle, A., & Yuen, J. (2007). Identification and mapping of lr3 and a linked leaf rust resistance gene in durum wheat. *Crop Science*, *47*(4), 1459–1466. https://doi.org/10.2135/cropsci2006.10.0663

Hiebert, C. W., Moscou, M. J., Hewitt, T., Steuernagel, B., Hernández-Pinzón, I., Green, P., Pujol, V., Zhang, P., Rouse, M. N., Jin, Y., McIntosh, R. A., Upadhyaya, N., Zhang, J., Bhavani, S., Vrána, J., Karafiátová, M., Huang, L., Fetch, T., Doležel, J., … Spielmeyer, W. (2020). Stem rust resistance in wheat is suppressed by a subunit of the mediator complex. *Nature Communications*, *11*(1), 1123. https://doi.org/10.1038/s41467-020-14937-2

Hiebert, C. W., Thomas, J. B., McCallum, B. D., Humphreys, D. G., DePauw, R. M., Hayden, M. J., Mago, R., Schnippenkoetter, W., & Spielmeyer, W. (2010). An introgression on wheat chromosome 4dl in rl6077 (thatcher*6/pi 250413) confers adult plant resistance to stripe rust and leaf rust (lr67). *Theoretical and Applied Genetics*, *121*(6), 1083–1091. https://doi.org/10.1007/s00122-010-1373-y

Huang, M., Liu, X., Zhou, Y., Summers, R. M., & Zhang, Z. (2018). Blink: A package for the next level of genome-wide association studies with both individuals and markers in the millions. *GigaScience*, *8*(2), giy154. https://doi.org/10.1093/gigascience/giy154

Huang, S., Liu, S., Zhang, Y., Xie, Y., Wang, X., Jiao, H., Wu, S., Zeng, Q., Wang, Q., Singh, R. P., Bhavani, S., Kang, Z., Wang, C., Han, D., & Wu, J. (2021). Genome-wide wheat 55k SNP-based mapping of stripe rust resistance loci in wheat cultivar shaannong 33 and their alleles frequencies in current chinese wheat cultivars and breeding lines. *Plant Disease*, *105*(4), 1048–1056. https://doi.org/10.1094/pdis-07-20-1516-re

Isidro, J., Akdemir, D., & Burke, J. (2016). Genomic selection. In A. William, B. Alain, & V. G. Maarten (Eds.), *The world wheat book: A history of wheat breeding* (Vol. 3, pp. 1001–1023). Lavoisier.

Jeger, M. J., & Viljanen-Rollinson, S. L. H. (2001). The use of the area under the disease-progress curve (AUDPC) to assess quantitative disease resistance in crop cultivars. *Theoretical and Applied Genetics*, *102*(1), 32–40. https://doi.org/10.1007/s001220051615

Joppa, L. R., & Williams, N. D. (1988). Langdon durum disomic substitution lines and aneuploid analysis in tetraploid wheat. *Genome*, *30*(2), 222–228. https://doi.org/10.1139/g88-038

Kaur, A., Sharma, A., Madhu, Verma, P. C., & Upadhyay, S. K. (2022). Ef-hand domain-containing proteins in *Triticum aestivum*: Insight into their roles in stress response and signalling. *South African Journal of Botany*, *149*, 663–681. https://doi.org/10.1016/j.sajb.2022.06.059

Kaur, J., Bansal, U. K., Khanna, R., Saini, R. G., & Bariana, H. S. (2009). Molecular mapping of stem rust resistance in hd2009/wl711 recombinant inbred line population. *International Journal of Plant Breeding*, *3*, 28–33.

Kaur, S., Gill, H. S., Breiland, M., Kolmer, J. A., Gupta, R., Sehgal, S. K., & Gill, U. (2023). Identification of leaf rust resistance loci in a geographically diverse panel of wheat using genome-wide association analysis. *Frontiers in Plant Science*, *14*, 1090163. https://doi.org/10.3389/fpls.2023.1090163

Klymiuk, V., Haile, T., Ens, J., Wiebe, K., N'Diaye, A., Fatiukha, A., Krugman, T., Ben-David, R., Hübner, S., Cloutier, S., & Pozniak, C. J. (2023). Genetic architecture of rust resistance in a wheat (*Triticum turgidum*) diversity panel. *Frontiers in Plant Science*, *14*, 1145371. https://doi.org/10.3389/fpls.2023.1145371

Klymiuk, V., Yaniv, E., Huang, L., Raats, D., Fatiukha, A., Chen, S., Feng, L., Frenkel, Z., Krugman, T., Lidzbarsky, G., Chang, W., Jääskeläinen, M. J., Schudoma, C., Paulin, L., Laine, P., Bariana, H., Sela, H., Saleem, K., Sørensen, C. K., … Fahima, T. (2018). Cloning of the wheat yr15 resistance gene sheds light on the plant tandem kinase-pseudokinase family. *Nature Communications*, *9*(1), 3735. https://doi.org/10.1038/s41467-018-06138-9

Knox, R. E., Clarke, J. M., & DePauw, R. M. (2000). Dicamba and growth condition effects on doubled haploid production in durum wheat crossed with maize. *Plant Breeding*, *119*(4), 289–298.

Kthiri, D., Loladze, A., N'Diaye, A., Nilsen, K. T., Walkowiak, S., Dreisigacker, S., Ammar, K., & Pozniak, C. J. (2019). Mapping of genetic loci conferring resistance to leaf rust from three globally resistant durum wheat sources. *Frontiers in Plant Science*, *10*, 1247. https://doi.org/10.3389/fpls.2019.01247

Kumar, D., Kumar, A., Chhokar, V., Gangwar, O. P., Bhardwaj, S. C., Sivasamy, M., Prasad, S. V. S., Prakasha, T. L., Khan, H., Singh, R., Sharma, P., Sheoran, S., Iquebal, M. A., Jaiswal, S., Angadi, U. B., Singh, G., Rai, A., Singh, G. P., Kumar, D., & Tiwari, R. (2020). Genome-wide association studies in diverse spring wheat panel for stripe, stem, and leaf rust resistance. *Frontiers in Plant Science*, *11*, 748. https://doi.org/10.3389/fpls.2020.00748

Kumar, S., Bhardwaj, S. C., Gangwar, O. P., Sharma, A., Qureshi, N., Kumaran, V. V., Khan, H., Prasad, P., Miah, H., Singh, G. P., Sharma, K., Verma, H., Forrest, K. L., Trethowan, R. M., Bariana, H. S., & Bansal, U. K. (2021). Lr80: A new and widely effective source of leaf rust resistance of wheat for enhancing diversity of resistance among modern cultivars. *Theoretical and Applied Genetics*, *134*(3), 849–858. https://doi.org/10.1007/s00122-020-03735-5

Lakkakula, I. P., Kolmer, J. A., Sharma, R., St. Amand, P., Bernardo, A., Bai, G., Ibrahim, A., Bowden, R. L., Carver, B. F., Boehm, J. D., & Aoun, M. (2025). Identification of leaf rust resistance loci in hard winter wheat using genome-wide association mapping. *The Plant Genome*, *18*(1), e20546. https://doi.org/10.1002/tpg2.20546

Larsson, S. J., Lipka, A. E., & Buckler, E. S. (2013). Lessons from dwarf8 on the strengths and weaknesses of structured association mapping. *PLoS Genetics*, *9*(2), e1003246. https://doi.org/10.1371/journal.pgen.1003246

Lebrec, J. J., Huizinga, T. W., Toes, R. E., Houwing-Duistermaat, J. J., & van Houwelingen, H. C. (2009). Integration of gene ontology pathways with North American Rheumatoid Arthritis Consortium genome-wide association data via linear modeling. *BMC Proceedings*, *3*(Suppl7), S94. https://doi.org/10.1186/1753-6561-3-S7-S94

Liu, W., Maccaferri, M., Bulli, P., Rynearson, S., Tuberosa, R., Chen, X., & Pumphrey, M. (2016). Genome-wide association mapping for seedling and field resistance to *Puccinia striiformis* f. sp. tritici in elite durum wheat. *Theoretical and Applied Genetics*, *130*(4), 649–667. https://doi.org/10.1007/s00122-016-2841-9

Maccaferri, M., Harris, N. S., Twardziok, S. O., Pasam, R. K., Gundlach, H., Spannagl, M., Ormanbekova, D., Lux, T., Prade, V. M., Milner, S. G., Himmelbach, A., Mascher, M., Bagnaresi, P., Faccioli, P., Cozzi, P., Lauria, M., Lazzari, B., Stella, A., Manconi, A., … Cattivelli,

L. (2019). Durum wheat genome highlights past domestication signatures and future improvement targets. *Nature Genetics*, *51*(5), 885–895. https://doi.org/10.1038/s41588-019-0381-3

Magwanga, R. O., Lu, P., Kirungu, J. N., Lu, H., Wang, X., Cai, X., Zhou, Z., Zhang, Z., Salih, H., Wang, K., & Liu, F. (2018). Characterization of the late embryogenesis abundant (LEA) proteins family and their role in drought stress tolerance in upland cotton. *BMC Genetics*, *19*(1), 6. https://doi.org/10.1186/s12863-017-0596-1

Mahmood, Z., Ali, M., Mirza, J. I., Fayyaz, M., Majeed, K., Naeem, M. K., Aziz, A., Trethowan, R., Ogbonnaya, F. C., Poland, J., Quraishi, U. M., Hickey, L. T., Rasheed, A., & He, Z. (2022). Genome-wide association and genomic prediction for stripe rust resistance in synthetic-derived wheats. *Frontiers in Plant Science*, *13*, 788593. https://doi.org/10.3389/fpls.2022.788593

Martínez-Moreno, F., Solís, I., Noguero, D., Blanco, A., Özberk, İ., Nsarellah, N., Elias, E., Mylonas, I., & Soriano, J. M. (2020). Durum wheat in the Mediterranean Rim: Historical evolution and genetic resources. *Genetic Resources and Crop Evolution*, *67*(6), 1415–1436. https://doi.org/10.1007/s10722-020-00913-8

McCartney, C. A., Somers, D. J., McCallum, B. D., Thomas, J., Humphreys, D. G., Menzies, J. G., & Brown, P. D. (2005). Microsatellite tagging of the leaf rust resistance gene lr16 on wheat chromosome 2bsc. *Molecular Breeding*, *15*(4), 329–337. https://doi.org/10.1007/s11032-004-5948-7

McIntosh, R., Wellings, C., & Park, R. (1995). *Wheat rusts: An atlas of resistance genes*. CSIRO Publishing. https://doi.org/10.1071/9780643101463

McMaster, G. S. (1997). Growing degree-days: One equation, two interpretations. *Agricultural and Forest Meteorology*, *87*(4), 291–300. https://doi.org/10.1016/S0168-1923(97)00027-0

Meuwissen, T. H. E., Hayes, B. J., & Goddard, M. E. (2001). Prediction of total genetic value using genome-wide dense marker maps. *Genetics*, *157*(4), 1819–1829. https://doi.org/10.1093/genetics/157.4.1819

Montalbini, P. (1992). Ureides and enzymes of ureide synthesis in wheat seeds and leaves and effect of allopurinol on *Puccinia recondita* f. sp. *tritici* infection. *Plant Science*, *87*(2), 225–231. https://doi.org/10.1016/0168-9452(92)90154-E

Montalbini, P. (1995). Effect of rust infection on purine catabolism enzyme levels in wheat leaves. *Physiological and Molecular Plant Pathology*, *46*(4), 275–292. https://doi.org/10.1006/pmpp.1995.1022

Mottaleb, K. A., Kruseman, G., Frija, A., Sonder, K., & Lopez-Ridaura, S. (2023). Projecting wheat demand in China and India for 2030 and 2050: Implications for food security. *Frontiers in Nutrition*, *9*, 1077443. https://doi.org/10.3389/fnut.2022.1077443

Pérez, P., & de los Campos, G. (2014). Genome-wide regression and prediction with the bglr statistical package. *Genetics*, *198*(2), 483–495. https://doi.org/10.1534/genetics.114.164442

Pakeerathan, K., Bariana, H., Qureshi, N., Wong, D., Hayden, M., & Bansal, U. (2019). Identification of a new source of stripe rust resistance yr82 in wheat. *Theoretical and Applied Genetics*, *132*(11), 3169–3176. https://doi.org/10.1007/s00122-019-03416-y

Pedersen, T. L. (2024a). ggraph: An Implementation of Grammar of Graphics for Graphs and Networks (R Package Version 2.2.1) [Computer software]. CRAN.

Pedersen, T. L. (2024b). tidygraph: A Tidy API for Graph Manipulation (R Package Version 1.3.1) [Computer software]. CRAN.

Prasad, P., Savadi, S., Bhardwaj, S., & Gupta, P. (2020). The progress of leaf rust research in wheat. *Fungal Biology*, *124*(6), 537–550. https://doi.org/10.1016/j.funbio.2020.02.013

Qi, T. (2017). Taarpc3, contributes to wheat resistance against the stripe rust fungus. *Frontiers in Plant Science*, *8*, 1245. https://doi.org/10.3389/fpls.2017.01245

Qiao, L., Gao, X., Jia, Z., Liu, X., Wang, H., Kong, Y., Qin, P., & Yang, B. (2024). Identification of adult resistant genes to stripe rust in wheat from southwestern China based on GWAS and WGCNA analysis. *Plant Cell Reports*, *43*(3), 67. https://doi.org/10.1007/s00299-024-03148-4

R Core Team. (2024). *R: A language and environment for statistical computing*. R Foundation for Statistical Computing. https://www.R-project.org/

Randhawa, M. S., Bariana, H. S., Mago, R., & Bansal, U. K. (2015). Mapping of a new stripe rust resistance locus Yr57 on chromosome 3BS of wheat. *Molecular Breeding*, *35*(2), 65. https://doi.org/10.1007/s11032-015-0270-0

Rosa, S. B., Zanella, C. M., Hiebert, C. W., Brûlé-Babel, A. L., Randhawa, H. S., Shorter, S., Boyd, L. A., & McCallum, B. D. (2019). Genetic characterization of leaf and stripe rust resistance in the Brazilian wheat cultivar toropi. *Phytopathology*, *109*(10), 1760–1768. https://doi.org/10.1094/PHYTO-05-19-0159-R

Rutkoski, J. E., Poland, J. A., Singh, R. P., Huerta-Espino, J., Bhavani, S., Barbier, H., Rouse, M. N., Jannink, J., & Sorrells, M. E. (2014). Genomic selection for quantitative adult plant stem rust resistance in wheat. *The Plant Genome*, *7*(3). https://doi.org/10.3835/plantgenome2014.02.0006

Sadeghabad, A. A., Dadkhodaie, A., Heidari, B., Razi, H., & Mostowfizadeh-Ghalamfarsa, R. (2017). Microsatellite markers for the *Triticum timopheevi*-derived leaf rust resistance gene lr18 on wheat 5bl chromosome. *Breeding Science*, *67*(2), 129–134. https://doi.org/10.1270/jsbbs.16148

Sapkota, S., Hao, Y., Johnson, J., Buck, J., Aoun, M., & Mergoum, M. (2019). Genome-wide association study of a worldwide collection of wheat genotypes reveals novel quantitative trait loci for leaf rust resistance. *The Plant Genome*, *12*(3), 1–14. https://doi.org/10.3835/plantgenome2019.05.0033

Savary, S., Willocquet, L., Pethybridge, S. J., Esker, P., McRoberts, N., & Nelson, A. (2019). The global burden of pathogens and pests on major food crops. *Nature Ecology & Evolution*, *3*(3), 430–439.

Sharma, R., Wang, M., Chen, X., Lakkakula, I. P., Amand, P. S., Bernardo, A., Bai, G., Bowden, R. L., Carver, B. F., Boehm, J. D., & Aoun, M. (2025). Genome-wide association mapping for the identification of stripe rust resistance loci in US hard winter wheat. *Theoretical and Applied Genetics*, *138*(4), 67. https://doi.org/10.1007/s00122-025-04858-3

Singh, R. P., Mujeeb-Kazi, A., & Huerta-Espino, J. (1998). Lr46: A gene conferring slow-rusting resistance to leaf rust in wheat. *Phytopathology*, *88*(9), 890–894. https://doi.org/10.1094/PHYTO.1998.88.9.890

Solh, M. B., Nazari, K., Tadesse, W., & Wellings, C. R. (2012). The growing threat of stripe rust worldwide. https://api.semanticscholar.org/CorpusID:155093700

Somers, D. J., Banks, T., DePauw, R., Fox, S., Clarke, J., Pozniak, C., & McCartney, C. (2007). Genome-wide linkage disequilibrium analysis in bread wheat and durum wheat. *Genome*, *50*(6), 557–567. https://doi.org/10.1139/g07-031

Spanic, V., Vukovic, A., Cseplo, M., Vukovic, R., Buchvaldt Amby, D., Cairo Westergaard, J., Puskas, K., & Roitsch, T. (2023). Early leaf responses of cell physiological and sensor-based signatures reflect susceptibility of wheat seedlings to infection by leaf rust. *Physiologia Plantarum*, *175*(4), e13990. https://doi.org/10.1111/ppl.13990

Spindel, J. E., Begum, H., Akdemir, D., Collard, B., Redoña, E., Jannink, J.-L., & McCouch, S. (2016). Genome-wide prediction models that incorporate de novo GWAS are a powerful new tool for tropical rice improvement. *Heredity*, *116*(4), 395–408. https://doi.org/10.1038/hdy.2015.113

Talebi, R., Mahboubi, M., Naji, A. M., & Mehrabi, R. (2023). Physiological specialization of *Puccinia triticina* and genome-wide association mapping provide insights into the genetics of wheat leaf rust resistance in Iran. *Scientific Reports*, *13*(1), 4398. https://doi.org/10.1038/s41598-023-31559-y

Tang, X., Xie, M., Kim, Y. J., Zhou, J., Klessig, D. F., & Martin, G. B. (1999). Overexpression of Pto activates defense responses and confers broad resistance. *The Plant Cell*, *11*(1), 15–29. https://doi.org/10.1105/tpc.11.1.15

The Gene Ontology Consortium, Aleksander, S. A., Balhoff, J., Carbon, S., Cherry, J. M., Drabkin, H. J., Ebert, D., Feuermann, M., Gaudet, P., Harris, N. L., Hill, D. P., Lee, R., Mi, H., Moxon, S., Mungall, C. J., Muruganugan, A., Mushayahama, T., Sternberg, P. W., Van Auken, K., Ramsey, J., … Ruzicka, L. (2023). The gene ontology knowledgebase in 2023. *Genetics*, *224*(1), iyad031. https://doi.org/10.1093/genetics/iyad031

The UniProt Consortium. (2022). UniProt: The universal protein knowledgebase in 2023. *Nucleic Acids Research*, *51*(D1), D523–D531. https://doi.org/10.1093/nar/gkac1052

Thompson, P., & Silverman, J. (2008). *The concept of accumulation in calculus*. The Mathematical Association of America. https://doi.org/10.5948/UPO9780883859759.005

Tong, J., Zhao, C., Liu, D., Jambuthenne, D. T., Sun, M., Dinglasan, E., Periyannan, S. K., Hickey, L. T., & Hayes, B. J. (2024). Genome-wide atlas of rust resistance loci in wheat. *Theoretical and Applied Genetics*, *137*(8), 179. https://doi.org/10.1007/s00122-024-04689-8

Tsilo, T. J., Kolmer, J. A., & Anderson, J. A. (2014). Molecular mapping and improvement of leaf rust resistance in wheat breeding lines. *Phytopathology*, *104*(8), 865–870. https://doi.org/10.1094/PHYTO-10-13-0276-R

VanRaden, P. (2008). Efficient methods to compute genomic predictions. *Journal of Dairy Science*, *91*(11), 4414–4423. https://doi.org/10.3168/jds.2007-0980

Wang, H., Zou, S., Li, Y., Lin, F., & Tang, D. (2020). An ankyrin-repeat and WRKY-domain-containing immune receptor confers stripe rust resistance in wheat. *Nature Communications*, *11*(1), 1353. https://doi.org/10.1038/s41467-020-15139-6

Wang, J. (2024). GAPIT: GAPIT (Genomic Association and Prediction Integrated Tool) (R Package Version 3.4.0) [Computer software]. GitHub.

Wellings, C. R. (2011). Global status of stripe rust: A review of historical and current threats. *Euphytica*, *179*(1), 129–141. https://doi.org/10.1007/s10681-011-0360-y

Wickham, H. (2016). *ggplot2: Elegant graphics for data analysis*. Springer. https://ggplot2.tidyverse.org

Wickham, H., François, R., Henry, L., Müller, K., & Vaughan, D. (2023). dplyr: A grammar of data manipulation (R Package Version 1.1.4) [Computer software]. CRAN.

Wu, N., Jiang, W., Xiang, Z., Asghar, R., & Akkaya, M. S. (2025). Assessment of self-activation and inhibition of wheat coiled-coil domain containing nlr immune receptor yr10cg. *Plants*, *14*(2), 278. https://doi.org/10.3390/plants14020278

Yao, F., Guan, F., Duan, L., Long, L., Tang, H., Jiang, Y., Li, H., Jiang, Q., Wang, J., Qi, P., Kang, H., Li, W., Ma, J., Pu, Z., Deng, M., Wei, Y., Zheng, Y., Chen, X., & Chen, G. (2021). Genome-wide association analysis of stable stripe rust resistance loci in a Chinese wheat landrace panel using the 660k SNP array. *Frontiers in Plant Science*, *12*, 783830. https://doi.org/10.3389/fpls.2021.783830

Yildirim-Ersoy, F., Ridout, C. J., & Akkaya, M. S. (2011). Detection of physically interacting proteins with the cc and nb-arc domains of a putative yellow rust resistance protein, yr10, in wheat. *Journal of Plant Diseases and Protection*, *118*(3–4), 119–126. https://doi.org/10.1007/BF03356391

Yin, L., Zhang, H., Tang, Z., Xu, J., Yin, D., Zhang, Z., Yuan, X., Zhu, M., Zhao, S., Li, X., & Liu, X. (2021). rmvp: A memory-efficient, visualization-enhanced, and parallel-accelerated tool for genome-wide association study. *Genomics, Proteomics & Bioinformatics*, *19*(4), 619–628. https://doi.org/10.1016/j.gpb.2020.10.007

Zhang, P., Li, X., Gebrewahid, T.-W., Liu, H., Xia, X., He, Z., Li, Z., & Liu, D. (2019). QTL mapping of adult-plant resistance to leaf and stripe rust in wheat cross sw 8588/thatcher using the wheat 55k SNP array. *Plant Disease*, *103*(12), 3041–3049. https://doi.org/10.1094/PDIS-02-19-0380-RE

Zhang, P., Yan, X., Gebrewahid, T.-W., Zhou, Y., Yang, E., Xia, X., He, Z., Li, Z., & Liu, D. (2021). Genome-wide association mapping of leaf rust and stripe rust resistance in wheat accessions using the 90k SNP array. *Theoretical and Applied Genetics*, *134*(4), 1233–1251. https://doi.org/10.1007/s00122-021-03769-3

Zhang, Q., Wei, W., Zuansun, X., Zhang, S., Wang, C., Liu, N., Qiu, L., Wang, W., Guo, W., Ma, J., Peng, H., Hu, Z., Sun, Q., & Xie, C. (2021). Fine mapping of the leaf rust resistance gene lr65 in spelt wheat 'altgold'. *Frontiers in Plant Science*, *12*, 666921. https://doi.org/10.3389/fpls.2021.666921

Zou, J., Semagn, K., Chen, H., Iqbal, M., Asif, M., N'Diaye, A., Navabi, A., Perez-Lara, E., Pozniak, C., Yang, R.-C., Graf, R. J., Randhawa, H., & Spaner, D. (2017). Mapping of QTLs associated with resistance to common bunt, tan spot, leaf rust, and stripe rust in a spring wheat population. *Molecular Breeding*, *37*(12), 144. https://doi.org/10.1007/s11032-017-0746-1

SUPPORTING INFORMATION

Additional supporting information can be found online in the Supporting Information section at the end of this article.

How to cite this article: Menor de Gaspar, J., Domínguez Rondón, A., García-Abadillo, J., Knox, R., Bokore, F. E., Boyle, K., Ammar, K., Huerta-Espino, J., Berraies, S., Meyer, B., Zhang, W., Cuthbert, R. D., Pierre, F., Ruan, Y., & Isidro y Sánchez, J. (2025). Mapping novel yellow and leaf rust loci and predicting resistance in cross derived Canadian durum wheat. *The Plant Genome*, *18*, e70124. https://doi.org/10.1002/tpg2.70124